KTH ROYAL INSTITUTE
OF TECHNOLOGY

Licentiate Thesis in Chemistry

Holistic evaluation and testing of coil coatings

ALEXANDER WÄRNHEIM

Stockholm, Sweden 2023

Holistic evaluation and testing of coil coatings

ALEXANDER WÄRNHEIM

Academic Dissertation which, with due permission of the KTH Royal Institute of Technology, is submitted for public defence for the Degree of Licentiate of Engineering on Monday 12th June 10:00 D37 Lindstedtsvägen 5, Stockholm.

Licentiate Thesis in Chemistry
KTH Royal Institute of Technology
Stockholm, Sweden 2023

ISBN 978-91-8040-570-6
TRITA-CBH-FOU-2023:20

Printed by: Universitetsservice US-AB, Sweden 2023

Abstract

Coil coatings are durable organic coatings used to protect metal sheets from corrosion and improve their aesthetic properties. Because of their extensive use, coil coatings have long been of interest for industrial and academic researchers. This interest has recently been furthered by a societal push towards the replacement of fossil-based raw materials with alternatives that are biobased and renewable.

The aim of this licentiate thesis is to demonstrate how analyses on the macro-, micro-, and nanoscale can be used to better understand the degradation process of polyester-based coil coatings. The included manuscripts showcase methods for evaluating and comparing different coil coating formulations and for verifying accelerated weathering techniques.

Multiple techniques, focusing on infrared (IR) spectroscopy and atomic force microscopy (AFM), were used to analyze coating systems before and after different types of weathering. IR data acquired from techniques without spatial resolution, such as attenuated total reflection (ATR) and photoacoustic spectroscopy (PAS) have been expanded upon with spatially resolved focal plane array (FPA) and s-SNOM (scattering-type scanning near-field optical microscopy) measurements. Spatially resolved chemical data of coating cross sections were acquired and used to assess how the degradation at the surface and in the bulk was related. Additionally, differences between the degradation behavior of a standard fossil-based coating and a similar coating with biobased components as well as differences between the degradation caused by artificial and natural weathering was discussed.

Nanoscale mechanical measurements of simplified coating surfaces showed that weathering increased nanomechanical stiffness and led to homogenization of mechanical properties on the local level. In addition, measurements with nanoscale FTIR correlated with macroscale FTIR. Even relatively minor changes in band intensities could be tracked on a local scale. Although the simplified samples were chemically homogeneous, nanoscale FTIR shows great promise for the assessment of local degradation of full systems.

Keywords:
Anti-corrosion coatings; Coil coating; Weathering; FTIR; nano-FTIR; Hyperspectral imaging; AFM; Nanomechanical properties

Sammanfattning

Bandlackering är en process för att applicera stabila organiska beläggningar på metallytor för att skydda från korrosion och förbättra deras utseende. På grund av beläggningarnas omfattande användning så har utvärdering och analys av dem varit av intresse för både akademi och industri i flera årtionden. Detta långvariga intresse har ytterligare främjats av en ökade miljömedvetenhet och ett tryck att ersätta miljöfarliga och fossila råmaterial mot biobaserade och förnyelsebara alternativ.

Målet med denna licentiatavhandling är att visa hur analysmetoder på makro-, mikro-, och nanonivå kan användas för att bättre förstå nedbrytning av bandlackerade beläggningar. Denna förståelse kan användas både för att utvärdera prestandan hos både nya redan befintliga system, men också för att kunna verifiera accelererade testmetoder vars mål är att minska tiden som krävs för utvärdering.

Flera tekniker, med fokus på infraröd (IR) spektroskopi och atomkrafts-mikroskopi (AFM) använts för att analysera beläggningar före och efter att de blivit utsatta för olika typer av aggressiva miljöer. Spektroskopiska data utan spatial upplösning som attenuerad totalreflektions FTIR (ATR) och fotoakustisk spektroskopi (PAS) har kompletterats med spatialt upplösta fokalplans array (FPA) och s-SNOM mätningar. Kemisk information med spatial upplösning har använts för att utvärdera hur nedbrytningen nära ytan relaterade till nedbrytningen längre ner i beläggningen. Likheter och skillnader i nedbrytningen som skedde i en standardbeläggning och ett system med biobaserade additiv jämfördes efter både väderbestendighets-testning som skedde utomhus och i labb. Skillnader mellan dessa exponeringsmetoder diskuterades också.

Nanomekanisk analys med hjälp av atomkraftsmikroskopi användes för att bestämma lokala förändringar av mekaniska egenskaper i förenklade klarlacker. Mätningarna visade att exponeringar i aggressiva miljöer leder till en lokal homogenisering av mekaniska egenskaper och ökad styvhet. Utöver detta så utvärderades likheter och skillnader mellan FTIR spektra som tagits på makro- och nanonivå. Dessa mätningar gav lovande resultat för fortsatta ytanalyser.

Nyckelord:
Korrosionsskyddsbeläggnignar, bandlackerade beläggningar, väderbeständighetstestning, FTIR, nano-FTIR, hyperspectral avbildning, Atomkraftsmikroskopi, nanomekaniska egenskaper

List of appended papers

Paper I. Depth-Resolved FTIR-ATR imaging studies of coating degradation during accelerated and natural weathering- Influence of biobased reactive diluents in polyester melamine coil coating
Wärnheim, A.; Edvinsson, C.; Sundell, P.-E.; Heydari, G.; Deltin, T.; Persson, D.
ACS Omega **2022**, *7* (27), 23842–23850.

Paper II Nanomechanical and nano-FTIR analysis of polyester coil coatings before and after artificial weathering experiments
Wärnheim, A.; Kotov N., Dobryden I., Telarietti Leggieri, R., Edvinsson C., Heydari G., Sundell P.-E., Deltin, T., Johnson C. M., Persson D., Claesson P. M.
Manuscript in preparation

Author contribution to the papers

Paper I
A majority of the experimental work. Part of the project planning. All of the data presentation and a majority of the analysis. A majority of manuscript preparation.

Paper II
Parts of the experimental work. A majority of the project planning. All of the data presentation and a majority of the data analysis. A majority of manuscript preparation.

Scientific contributions not included in the thesis

Polyester-melamine coil coating formulation reinforced with surface-modified cellulose nanofibrils
Telaretti Leggieri M.R., Deltin T., Wärnheim A., Sundell P.-E., Malmström E., and Johansson M.
Prog. Org. Coatings **2023**, *182*, 107608.

Abbreviations

AFM	atomic force microscopy
ATR	attenuated total reflection
CT	cyclic trimer
DMA	dynamic mechanical analysis
DMTA	dynamic mechanical thermal analysis
FPA	focal plane array
FTIR	Fourier transform infrared
GR	gloss retention
GU	gloss units
HDI	hexamethylene diisocyanate
HMMM	hexa(methoxymethyl)melamine
IR	infrared
IRE	internal reflection element
ISO	international organization for standardization
MCT	mercury cadmium telluride
MEP	moisture-enhanced photolysis
MSFL	melamine substitution functionality loss
OI	oxidative index
OPD	optical path difference
OPO	optical parametric oscillator
PAS	photoacoustic spectrometry
POI	photooxidative index
QCL	quantum cascade laser
RME	rapeseed methyl ester
s-SNOM	scattering-type scanning near-field optical microscopy
T_g	glass transition temperature
TOW	time of wetness
UV	ultraviolet
vdW	van det Waals
VOC	volatile organic compounds

Table of Contents

Introduction

Motivation

An ecologically sustainable society is defined by environmentally benign processes and products, where natural resources are used with great care. One important route towards less use of resources is to make materials that last longer, and, when possible, use renewable materials. Metals are key in our society. Metals are not renewable but can be recycled. Thus, for sustainability recycling is important. Likewise, it is important to provide for long lifetimes of metal products. To this end metals are often coated to provide barriers that counteract corrosion and wear. In addition, coatings are used to alter the aesthetic properties of the surface, adding colors and textures. A problem with organic coatings is that they also degrade with time. Thus, for prolonging the lifetime of metal objects one should also prolong the lifetime of organic coatings. This fact motivates investigations of coating degradation processes, where in particular the initial stages of coating degradation is relatively unexplored. This work contributes to fill some of the knowledge gaps in this area.

Aims

The aim of this project is to utilize advanced characterization techniques to measure and quantify local chemical and mechanical changes in coil coatings on top of metal substrates, and to elucidate how these changes are related to other coating properties. This will lead to increased understanding of the initial stages of coating degradation. It will also provide a better understanding of the results of accelerated aging and the effect of various exposure parameters such as relative humidity and temperature as well as incident light in terms of both intensity and wavelength. The information obtained is intended to facilitate the development and assessment of new coatings, e.g. with biobased more sustainable raw materials but also in evaluating similarities and differences between artificial and natural weathering.

Sustainable development goals

In 2015, all countries that are members of the United Nations agreed on a plan called the 2030 Agenda for Sustainable Development. This plan draws up 17 Sustainable Development Goals (SDGs) that aims to be the blueprint for peace and prosperity for people and the planet, now and into the future. These goals encourage all countries to work together to end poverty whilst improving health and education of the global population at the same time as it aids in reducing inequality and encouraging economic growth. Additionally, the plan emphasizes the need to address climate change and protect our natural resources, such as oceans and forests. Ultimately, the SDGs represent a global effort to create a peaceful and prosperous future for both people and the planet.

This research mainly aims to impact two of these SDGs; SDG 9 promoting sustainable industrialization and foster innovation and SDG 12 sustainable consumption and production. In terms of SDG 9, an increased understanding of degradation in coil coatings though the improvement of degradation measurement techniques aids the research and development in the formulation and production of new coatings. It would help to better optimize the durability of the systems, decreasing CO_2-emissions per year of usage of the products. For SDG 12, a longer lasting coating (and thus metal substrate) would decrease consumption of metals and reduce waste from replacing corroded or otherwise damaged coated panels. This contributes to the efficient usage of natural resources.

In addition, aiding in the development of new coating formulation potentially allows for a faster replacement of for fossil based and otherwise environmentally damaging materials. This is related to SDG 13, urgent action to combat climate change, by reducing the need for fossil based raw materials that contributes to global warming.

Background

Coil coatings

Coil coatings are a type of organic coating systems applied onto metal substrates in a continuous highly efficient process. Although they have a wide array of different applications in everything from metal roofing to appliances, the manufacturing process is usually relatively similar.

A typical manufacturing process starts with the unrolling of a coil of metal into an accumulator. The accumulator uses mobile blocks to store the metal sheet and release it gradually at a desired rate, keeping the feeder at the start stationary and the feeding rate of coil into the system constant. This allows multiple coils to be joined together without disturbing the continuous process. The metal sheet exiting the accumulator is cleaned, removing any oil or corrosion products from manufacturing and storage. It is then pretreated using a conversion coating to improve the adhesion between the metal and the organic coating and for passivation. Common conversion coatings include thin films pretreatments based on titanium or thicker zinc phosphate coatings.

After this initial step of preparing the metal substrate, an organic primer is applied using a roller coater. The primer coated metal sheet passes through an oven to remove any volatile compounds and cure the thermoset primer. Quenching using water or air is commonly used before the topcoat is applied using a second roller coater. The topcoat is then cured using a second oven, and quenched before it goes onto the second accumulator that allows for controlled re-rolling the metal sheet into a new coated coil of the desired size. The coil coating process is schematically shown in Figure 1.

This continuous and well-optimized process results in efficient and low waste production of large metal sheets (often steel or aluminum), compacted into easy-to-transport rolled up coils with high surface uniformity both in terms of aesthetic appearance, mechanical, and chemical properties. The production is seeing continuous development. Decades of research and development have resulted in different categories of systems with applications in everything from the white painted metal sheets that are mounted on the side of washing machines to paneling in buses.

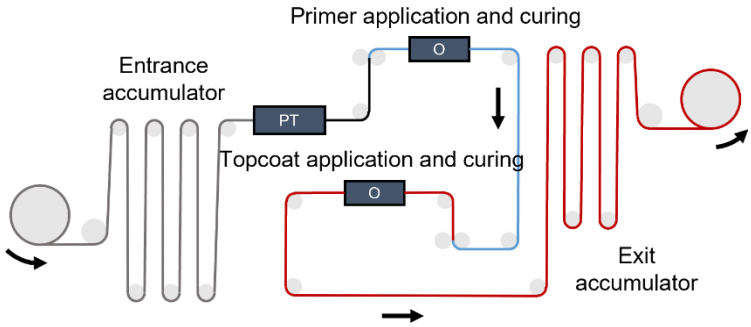

Figure 1. A schematic production line showing the coil coating process. Firstly, a dark gray metal coil is unrolled into the entrance accumulator. After this, pretreatment (PT) of the metal is done which is schematically shown as the metal turning black. Then, the primer is applied and cured in an oven (O), as shown in blue. After this, the topcoat application and curing are shown in red. Finally, the coated metal goes into the exit accumulator before it is recoiled.

The focus in this thesis lies on the characterization of degradation in the topcoat layer in polyester-based coil coatings. This outermost part of the coating is designed to prevent damage caused by an aggressive outdoor environment reaching into the rest of the coating, and further down to the metal substrate. To prevent this, the topcoat needs to retain its chemical and physical properties when exposed to harsh outdoor environments. In addition, from an end user perspective, it is also important to consider how the aesthetic properties are affected by these extreme conditions.

Chemistry of coil coatings

The chemical make-up of coil coatings is complex, and many different constituents are involved. These include among other things pigmentation such as carbon black or metal oxides, structural agents such as polyamide or PMMA to improve the mechanical properties and change the surface texture, and solvents such as different types of volatile organic compounds (VOC) to adjust the viscosity and curing. Recently, steps have been taken to reduce the amount of VOC in the manufacturing, replacing them with milder chemicals. One avenue that has been explored is reduction in the required amount of VOCs content with addition of hydroxy-functional hyper-branched polyester resin and a biobased reactive diluent, rapeseed methyl ester (RME) [1], [2].

To make meaningful generalizations it is often convenient to group the different systems based on resin and crosslinking agent. Two of the system types with the largest market share are polyester melamine and polyester

isocyanate. Polyester isocyanate is also sometimes called polyester urethane or PUR due the urethane bonds formed during crosslinking. Figure 2 shows a schematic of two typical crosslinkers, one melamine and one isocyanate, before and after they have been cured as to react with a polyester resin.

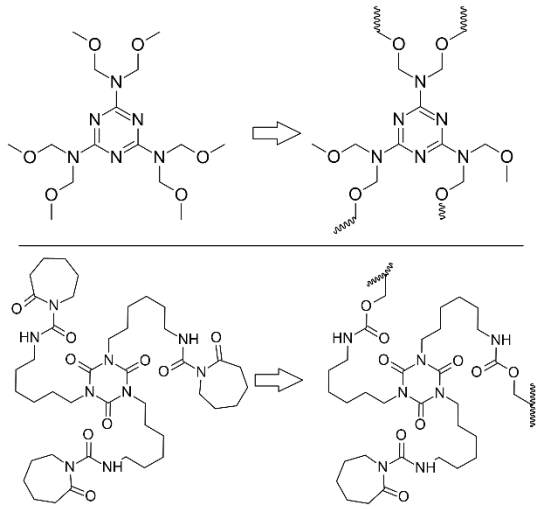

Figure 2. The molecular structure of hexa(methoxymethyl)melamine (HMMM) and caprolactam blocked hexamethylene diisocyanate (HDI) a cyclic trimer (CT) before (left) and after (right) a crosslinking reaction has taken place.

The ratio of resin to crosslinker is one example where the chemical balance of a coil coating system is important. If there are too few available active crosslinker sites, then only a limited amount of crosslinking can take place and the coil coating will be mechanically weak, but too much crosslinker also has a negative impact on the performance. For instance, the melamine in polyester melamine has shown preference for self-condensation at higher concentrations, increasing the temperature at which large scale molecular movements starts to occurs (T_g) and lowering the flexibility of the coating [3].

The curing step in the manufacturing process has a high impact on the diffusion of reactive species in these thermosets. It is important to strive to avoid both under curing and over curing. Under curing can result in a too soft coating with low degree of crosslinking, and it has also been shown to correlate with an increase of migration of low molecular compounds to the surface during weathering. Overcuring results in a high degree of

crosslinking, but also a coating that becomes (too) brittle. The main parameter used to quantify the curing temperature is called peak metal temperature, or PMT. This is the highest temperature that the metal substrate reaches during the curing process and at lower oven temperature it takes a longer time to reach PMT and vice versa. A higher oven temperature can result in faster reactions and shorter curing times. In general, a higher temperature is correlated with a faster curing reaction, resulting in higher T_g and a higher degree of crosslinking at a set curing time [4]. However, a lower oven temperature and a longer curing time often forms a better-connected network but might not be practical in industrial applications [5].

Regardless of how well optimized the curing conditions are, it has been shown using molecular dynamic simulations that crosslinked networks, especially those made by using crosslinker precursors with high functionality, can have a significant number of structural and topological imperfections [5]–[7]. These might cause macromolecular imperfections such as dangling ends or loops, or even voids. These imperfections can all have significant negative impact in coating performance and act as sites for defect initiation. It has been shown that local sites, measuring ~50 nm in diameter, with higher crosslinking and lower macroscopic density show an increased water uptake as compared to the surrounding areas in epoxy-phenolic coatings [8].

Degradation of coil coatings

When a coil coating is exposed to UV irradiation (as well as other parts of the electromagnetic spectra), humidity, and heat, their properties change and they tend to degrade. Visually this is often measured using a reduction in gloss and changes in color [9]–[11]. Mechanically it is typical that they become more brittle [9], [12].

On a chemical level, degradation of a coil coating can occur via different degradation modes triggered by a multitude of factors. Many of these modes rely on the presence of water. For example, hydrolysis can take place in ether linkages in both esters in a polymer matrix or in the arms of to the central triazine in a melamine crosslinker [12], [13]. A reaction scheme of the latter process is shown in Figure 3.

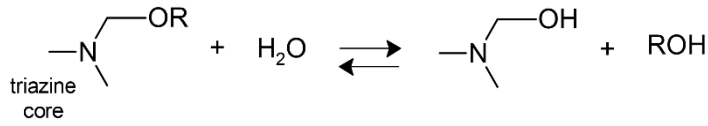

Figure 3. Hydrophilic breakdown of a polyester-melamine resin

In polyester isocyanate coil coatings, bonds in the urethane linkages can be broken resulting in separation of a R-OH group and the release of carbon dioxide [13].

Another factor affecting degradation is the absorption of incoming electromagnetic radiation, in particular in the UV-region. At a simplified level, a photon with sufficient energy has the possibility of cleaving a chemical bond and creating a radical. This radical has the possibility to e.g. abstract atoms from nearby molecules or linking with other radicals. A higher energy (lower wavelength) photon can break more stable bonds, which is why UV light is often the main consideration in the context of degradation. However other wavelengths such as visible and IR light can also greatly affect the degradation by for example causing increases in temperature in pigmented systems [14].

An example of a degradation reaction being triggered by UV light can be seen in polyester melamine after exposure to water. Methylol groups are formed due to hydrolysis of ether linkages in the system. When exposed to UV light the methylol will react and form an amine group attached to the melamine and a free formaldehyde molecule. The formaldehyde can react further, forming formyl and hydrogen free radicals, which in turn can abstract a hydrogen atom from surrounding polymer chains [12].

As described above, the chemical changes associated with degradation are often dependent on a combination of external factors. Therefore, it is not a surprise that the degradation is not just a sum of reactions triggered by the presence of water, reactions reliant on incoming UV radiation, and reactions caused by an elevation of temperatures. For example, degradation rates in melamine-formaldehyde and acrylic melamine systems exposed to simultaneous UV-radiation and humidity are higher than the sum of degradation caused by dry UV exposures and dark hydrolysis [15], [16]. Nguyen et al. have shown that increases in humidity speeds up the photolysis rate in a partially methylated melamine acrylic polymer, and called this phenomenon moisture-enhanced photolysis (MEP) [17].

Nguyen et al. has also showed the formation and growth of μm and nm scale pits in model coating formulations after accelerated weathering [18]. The weathering was performed using various combinations of humidity, UV dosage, and elevated temperatures and the holes where quantified using atomic force microscopy (AFM). They proposed the Nguyen-model that suggests that the coatings analyzed are chemically heterogeneous, consisting of hydrophilic domains interdispersed with crosslinked units. Thus, the degradation reactions do not occur homogeneously throughout the entire coating surface.

Analytical techniques

The ability to quantify the degradation in a coil coating and being able to understand what occurs when it is exposed to environmental stressors is important. Not only to gain a more fundamental understanding of polymer chemistry, but also to be able to evaluate coating performance. Highly accurate strategies to determine and quantify performance are needed in the development of new coatings with biobased raw materials with lower environmental impact as well as for the optimization of production parameters to decrease energy requirements.

Gloss retention

Gloss, or the ability of a surface to reflect light, is an important property for a coil coating. Although there is no direct correlation between the chemical state of a coating and the gloss, it has historically been used as a way to evaluate the degradation of coil coatings [19], [20]. Largely because gloss is relatively easy to measure, and that it greatly affects the appearance of the coating, making it noticeable to the end user.

The principle of gloss measurements is relatively simple. When incident light hits a reflective surface, it can either be reflected, refract into the sample or be absorbed. Reflected light can, depending on the refractive index and incident angle, either be reflected diffusely and scattered in all solid angles or be reflected in the main specular direction.

A typical gloss measurement uses gloss units (GU) to quantify how much of incoming light is being reflected in the main specular direction. GU are defined relative to a completely matte surface being equal to 0GU and a standard polished black glass reference being equal to 100GU. To make these measurements harmonize with gloss as perceived by the human eye they are taken at different incident angles. If the gloss is above 70 GU the incidence angle should be decreased and if the gloss level is below 10 GU it

should be increased. ISO 2813, and ASTM D523 are two of the most used standards in gloss measurements for coatings. They both prescribes that the incident angle of light used to measure gloss should be either 20°, 60°, and 85° with respect to a line perpendicular to the surface, as shown in Figure 4.

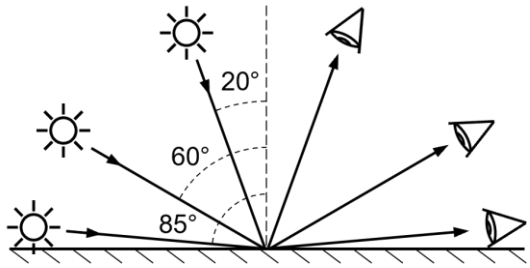

Figure 4. A representation of gloss measurements at 20° (high gloss surface), 60° (semigloss surface), and 85° (matt surface).

When comparing gloss before and after weathering it is common to use gloss retention (GR) which is calculated as a percentage according to eq. 1.

$$GR\ (\%) = 100\ \times \frac{G_{initial}}{G_{exposed}} \tag{1}$$

Where $G_{initial}$ is the initial gloss in gloss units and $G_{exposed}$ is the gloss after exposure.

DMA

A ubiquitous analysis method for determining viscoelastic properties of coatings is dynamic mechanical analysis (DMA), sometimes called dynamic mechanical thermal analysis (DMTA). During the measurement a sample is fastened into two clamps and subjected to sinusoidal deformation. The resulting stress and strain are measured over a range of temperatures. From this, two moduli are calculated, loss modulus and storage modulus, respectively, representing the viscous and the elastic part of the response of the sample. The ratio of loss modulus to storage modulus to is called tan δ and the temperature at which it reaches its the maximum value is defined as the glass transition temperature (T_g) of the sample. This is the temperature above which large scale molecular movements are possible and the material goes from a rigid state to a more flexible state.

Note that this is not a phase transition. In general, higher crystallinity and higher crosslinking is associated with a higher T_g.

T_g is a useful property in coating science since it has significant effects on the performance of a coating. Above T_g a coating is softer, more formable, and has a higher water uptake [21].

A practical problem with analyzing coil coating degradation using DMA is that it is very difficult to analyze a coating applied onto a metal substrate. This means that a free film needs to be manufactured and put in special sample holders, before weathering. In addition, weathering can lead to changes in the mechanical properties of the films and lead to mechanical failure. For example, if the free film is placed directly against a surface, the film can attach to the sample holder. That would make removal of the film for subsequent DMA measurements hard without causing significant damage. On the other hand, if the film is suspended into the air using tension it might start sagging and break. Narayan et al. 2004 and Mitra et al. 2014 are two examples of successful attempts to weather free films. Both noted that increasing weathering times resulted in an increase in T_g [13], [22].

Atomic force microscopy

A well-established way of acquiring high resolution surface information is atomic force microscopy (AFM), as introduced by Binning et al. 1986 [23]. In its simplest form it is based on a fine tip at the end of a cantilever. By measuring the path of a laser reflected off the top of the cantilever and using sensitive piezo electronics it is possible to closely monitor the position of the tip as it scans across the surface. These first machines measured the surface topography, but later improvements added a multitude of possibilities to determine different local surface properties.

One example of the applications of AFM in the field of coil coating analysis is Biggs et al. 2001 [24]. They investigated the topography of pigmented polyester melamine and found that the surface roughness increased with accelerated weathering. They suggested that the increase was related to removal of the outer coating layer, which in turn exposed hard pigments at the surface and even fell out of the coating.

Nanomechanical analysis

Nanomechanical measurements were pioneered by Colton and Burnham in 1989 [25]. In a typical topographical AFM measurement the tip only lightly touches the sample surface, or entirely remains out of contact. In contrast, nanomechanical measurements build on monitoring

the cantilever deflection as the tip is pushed into the sample, compressing it, and then is pulled out again, whereby allowing the material to decompress. The tip is then moved to the next area and the process is repeated. The vertical deflection of the tip and the position relative to the surface is monitored. A schematic illustration of the deflection-position curve during a typical nanomechanical measurement of a sample is shown in Figure 5.

At the start of the compression process, when the tip is far away from the sample the deflection is set to zero as there are no surface-tip interactions. As the tip approaches the surface, attractive forces often act upon the tip and increases in magnitude with decreasing tip-surface distance. This results in a decreasing cantilever deflection, resulting in negative values with increasing magnitude. As the tip approaches the surface, additional repulsive forces start acting and the magnitude of the deflection decreases. The point where the deflection goes back to zero is defined as the contact point, even though tip-sample contact could occur before this point. As the tip is pushed into the sample and compressing it the nearly linear portion of the slope at high forces denotes the compressive stiffness of the surface. At a certain point, the deflection reaches a pre-determined maximum value, the peak force, and the tip starts to retract and now decompression of the sample is initiated.

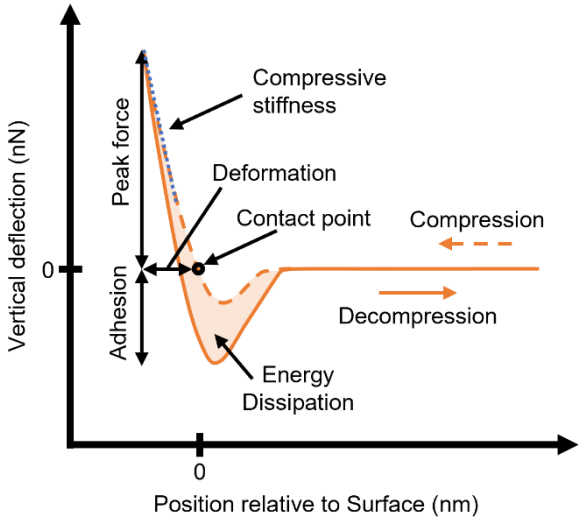

Figure 5. Schematic representation of a compression-decompression curve in Peak Force AFM.

The physical distance between the contact point and the point at which the peak force was achieved is often reported as the deformation of the sample. The linear slope during the early stages of decompression is sometimes reported and is then denoted as the decompressive stiffness. As the tip is further retraced and leaves the sample, attractive forces give rise to negative deflection, until the tip is retracted out of the range of these forces. The magnitude of the largest negative deflection during the decompression is the adhesion force. Sudden jumps in the deflection curve could indicate the presence of bridging polymer chains that gradually lose contact with the tip, or capillary forces and breaking of the water meniscus or motion by the three-phase contact line along the surface [26]–[28].

Each compression-decompression cycle can take less than a millisecond. In case the compression-decompression curve overlap, except for the adhesive region that cannot be explored on approach, the deformation is elastic and the Young's modulus can be extracted using a proper contact mechanics model [29]. However, if the surface of the analyzed sample is viscoelastic fast cycles might not allow the material to relax, thus creating hysteresis in the deflection-position curve. In such a case, one may report and apparent elastic modulus, but this modulus will depend on the measurement speed [30], [31]. Note that the stiffness and Young's modulus for coil coatings are measured using deformations in the nm range, which makes the analysis very surface sensitive [32].

Infrared spectroscopy

Vibrational modes represent quantized vibrational energy states in a molecule characteristic for specific molecular bonds. Incident energy in the form of electromagnetic radiation of one or more wavelengths can cause a transition from a lower energy mode to a higher one. Since the energy levels are quantized, only certain wavelengths are absorbed, typically from the infrared part of the electromagnetic spectrum. By determining which energies that are absorbed it is possible to determine the presence of certain chemical bonds, and therefore the present molecules. This is the basis of infrared (IR) spectroscopy.

By convention, the spectral data is usually presented as the absorbance or transmission as a function of wavenumber, with the wavenumber being the inverse of the wavelength. There are two main approaches to creating these spectra. The first one is by recording absorbance at a small part of the spectra at the time, gradually changing the incident (and therefore absorbed) wavenumber and recording absorbance at each point. This has

historically been done using a dispersive spectrometer or more recently using a tunable quantum cascade laser (QCL). A dispersive spectrometer utilizes optics to separate different wavenumbers from a broadband infrared source. A QCL is a type of semiconductor laser with a considerably higher scan rate and energy in comparison to for example tunable optical parametric oscillator (OPO) lasers. However, it also comes with a more limited spectral range and generally a higher price tag. The second approach is to use a broadband IR source in combination with a Michelson interferometer, after which the data is transformed into a spectrum using a Fourier transform. Hence the name Fourier transform infrared (FTIR) spectroscopy. In its simplest form a Michelson interferometer consists of a light source, a beamsplitter, a stationary mirror, and a moving mirror, the sample, and a detector. The beamsplitter separates the incoming light and lets some radiation go to the stationary and some to the moving mirror. The light is then reflected from the mirrors and is recombined before it interacts with the sample and is refocused on the detector. The movement of the mirror causes an optical path difference (OPD), or a difference in how far the two beams of light travel. This leads to a constructive and destructive interference, with the light intensity being dependent on the mirror position. From this, an interferogram can be created, which in turn can be translated into a conventional spectrum using a Fourier transformation. FTIR is the most common method of doing IR-based measurements as it allows for rapid collection of information from a wide spectral range. A simple schematic of a Michelson interferometer and a FTIR transmission measurement is shown in Figure 6.

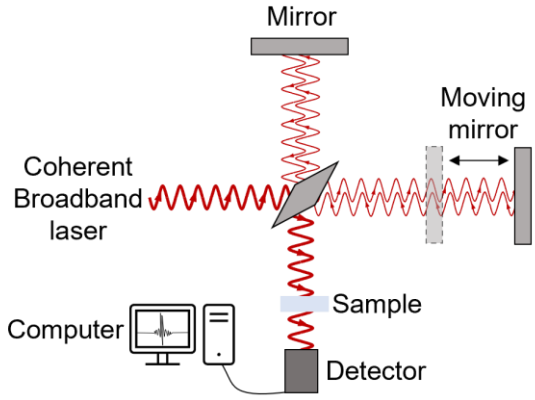

Figure 6. A schematic FTIR transmission measurement using a Michelson interferometer.

Attenuated total reflection

ATR (attenuated total reflection) is one of the most well-established methods for collecting chemical information from organic coatings [33], [34]. Two of the most important reasons behind the wide-spread usage is that the technique is relatively straightforward to use and most of the time require little sample preparation [35].

An internal reflection element (IRE), transparent to IR light is brought into contact with a sample surface. Then IR light is shone into the IRE, and total reflection occurs at the sample-IRE interface. After this, the light is led into a detector. To achieve this, the IRE material must have a refractive index high enough to result in total internal reflection when in contact with a sample. The refractive index needed to provide total reflection is given by Snell's law in eq. 2.

$$\theta_c = \sin^{-1}\left(\frac{n_2}{n_1}\right) \tag{2}$$

With θ_c being the critical angle, or the smallest angle required for total reflection, n_1 the refractive index of the IRE, and n_2 the refractive index of the sample. A typical value for refractive index of polymers and organic coatings in the mid IR region is 1.5 [20], [35]. Typical IRE materials include Diamond and germanium, with refractive indexes of 2.38 and 4.00 in the mid IR region. Note that since total reflection occurs inside the IRE, the beam path of the light never extends into the sample. Instead, an electrical field, called an evanescent wave extends from the IRE-sample interface. The field strength decreases exponentially with distance, which means that information is only collected from the outermost layer of the coating. To quantify how far the wave reaches, depth of penetration, d_p is often used. This is the depth at which the field strength has decreased to e^{-1} ($\approx 37\%$) of the field strength at the interface and can be calculated using eq. 3 [35].

$$d_p = \frac{\lambda}{2\pi n_1 \left(\sin^2\theta - \left(\frac{n_2}{n_1}\right)^1\right)^{½}} \tag{3}$$

Where λ is the wavelength and θ is the incident angle of the incoming light, n_1 the refractive index of the IRE, and n_2 the refractive index of the sample.

Hirayama et al. used this principle, and by changing the angle of incident light they compared the degradation at the surface of a coil coating with the degradation further into the bulk [36]. Note that available IRE materials set the maximum penetration depth on the scale of a few µm.

Photoacoustic spectroscopy

A technique with a larger range of penetration depth customization is photoacoustic spectrometry FTIR (PAS), which build on the photoacoustic effect. Absorbance of IR light induce thermal vibrations, which propagate through the material. If the vibrations reach the surface, they continue out into the surrounding atmosphere, at which point they can be quantified using a microphone. A typical photoacoustic cell consists of a gastight container with an IR-transparent window, a sample holder, and a microphone as shown schematically in Figure 7. Practically, purging the chamber with a noble gas such as helium and minimizing humidity greatly increases the signal to noise ratio.

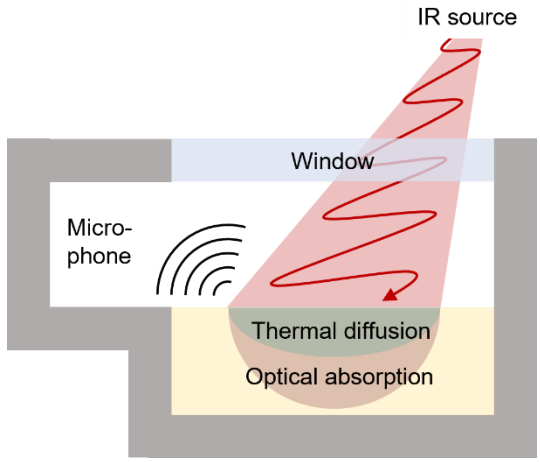

Figure 7. A schematic photoacoustic cell where the thermal diffusion length considerably smaller than the optical absorption depth

There are two main factors that decide the depth from which information is collected. How far into the material IR radiation can penetrate and how far the vibrations can travel through the material. The relationship between optical absorption, propagation of thermal vibrations, and the photoacoustic signal is complex. Thus, it is often convenient to make simplified suppositions about the material properties

to approximate the behavior of the material [37], [38]. These scenarios might include cases where the sample is completely optically transparent or where all light is absorbed at very narrow depths [35]. One of the most used approximations in the context of coating analysis is that the propagation of thermal waves is the limiting factor. The thermal wave decay length L, or the distance after which the signal intensity has decreased to e^{-1} ($\approx$ 37%) of the maximum intensity, can be calculated using eq. 4 [39]:

$$L = \left(\frac{D}{\pi f}\right)^{½} \tag{4}$$

Where D is the thermal diffusivity of the sample, and f is the modulation frequency of the incoming signal. The modulation frequency is in turn dependent on the rate at which the OPD (optical path difference) changes, as well as the wavenumber ($\tilde{v}$) and the optical velocity (V) according to $f = V \times \tilde{v}$. Using this correlation, it is possible to tune the thermal wave decay length by changing the optical velocity between different measurements.

The wavenumber-dependence of L has implications when it some to the evaluation of IR-spectra. For example, although L is affected when f changes, f does not affect the optical penetration depth. This means that when decreasing f it is possible to reach what is called optical saturation. Optical saturation occurs when the approximation that the propagation of thermal waves is the limiting factor in the measurement break down and L approaches the optical penetration depth. At this point, decreasing f further will not increase the information depth. Since L is also wavenumber-dependent different wavenumber regions of the spectra will reach optical saturation at different values of f.

The non-destructive nature of this technique and the tunability in penetration depth has made it a popular method for analyzing coatings. It is however limited in that detailed analysis requires both thermal and optical properties for the sample. These properties can be complicated to acquire from coatings already applied onto a metal substrate.

Zhang et al. has used PAS to assess multilayer coil coating systems with and without pigmentation at depths in the range 5 to 25 μm [40]. They concluded that the inorganic pigmentation increased the thermal diffusion

depth, thus complicating the assessment and making the calculated penetrations depths inaccurate.

Gonon et al. 2001 analyzed photooxidation of a polymer surface as a function of depth with both PAS and micro-FTIR, a combination of a microtome and transmission FTIR [41]. PAS was used to analyze the outermost layer, 5 – 35 μm from the surface, whereas the micro-FTIR was used to reach depths between 10 – 100 μm. They concluded that the two methods gave similar results at the overlapping depths, but PAS provided a considerably better depth resolution. In addition, the microtomation procedure could potentially cause smearing or other types of damage the sample.

An additional factor to consider with PAS analysis is that it is not spatially resolved. The entire surface volume contributes to the signal, which means that any local effects of degradation will be hidden. This is for example relevant when analyzing the effect pigmentation has on coating stability.

Focal plane array detectors

One method of acquiring spatially resolved molecular information is by combining an IR source with an array detector, making it possible to separate information from different parts of a sample. This is called FTIR focal plane array (FPA) imaging. A schematic FPA-reflection measurement is illustrated in Figure 8.

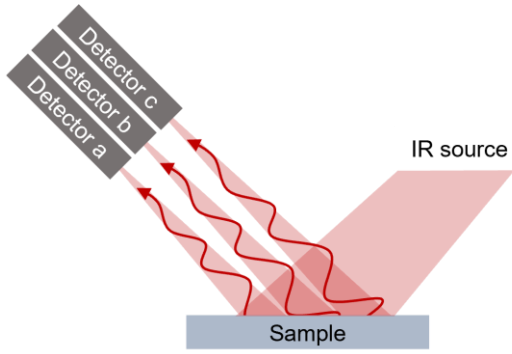

Figure 8. A schematic FTIR reflection measurement with a focal plane detector array

Like other far-field optical-based techniques the spatial resolution of this technique is diffraction limited. More specifically, the spatial resolution is limited by the wavelength of the infrared radiation, and the microscope optics according to Rayleigh's criterion (eq 5) [35]:

$$r = \frac{1.22\lambda}{2NA} \tag{5}$$

Where r is the distance between two resolvable points in space, λ is the wavelength, and NA is the numerical aperture of the microscope objective, equal to $n\sin(\theta)$.

IR wavelengths are relatively large, typically in the range of 2 -20 μm in the mid IR range, which limits the spatial resolution of the measurements. To achieve the best possible resolution, it is possible to add an IRE-accessory to an FTIR-FPA microscope, resulting in FTIR-FPA-ATR. For example, analyzing spectral region around 1550 cm^{-1} using a Ge IRE in a typical commercial coil coating system result in a theoretical spatial resolution around 2 μm according to Persson et al. 2020 [42]. However, practically the resolution has been determined to be closer to 3-4 μm due to optical aberrations [43].

In this thesis work FPA analysis was used to acquire depth resolved imaging of coil coating cross sections. This allowed for analysis and discussion of the relation between degradation occurring at the surface and in the bulk. Both the effect of different coating formulations as well as comparisons between different weathering scenarios were discussed.

Nanoscale IR spectroscopy

A way to further increase the resolution of IR spectroscopy is by combining it with AFM. Three commercially available approaches are available, all with a typical lateral resolution around 20 nm.

The first method s-SNOM (scattering-type scanning near-field optical microscopy) or also called nano-FTIR was used for measurements performed in Paper II. It is an optical technique independent of mechanical properties of the sample. To collect a spectrum from a specific point, a coherent broadband laser or QCL is focused on an AFM tip coated with a noble metal. This makes the tip work like an antenna, inducing a strong local electric near field confined under the tip apex that declines exponentially with distance [44]. Backscattering from the tip is continuously collected using interferometric detection. If the tip is brought

close to a sample the collected optical data contains information about the near field interaction between the tip and the sample [45]. In essence, the incoming electric field E is scattered and affected by both the refractive index n and extinction coefficient k of the tip and the sample. This is schematically shown in Figure 9. From this, the phase or imaginary part of the scattering coefficient can be translated into nano-FTIR absorption which has been shown to correlate with macroscale FTIR spectra [46]. With the addition of a QCL, it is also possible to use pseudo-detection to determine the intensity of a specific wavenumber region across a surface with a lateral resolution around 20 nm.

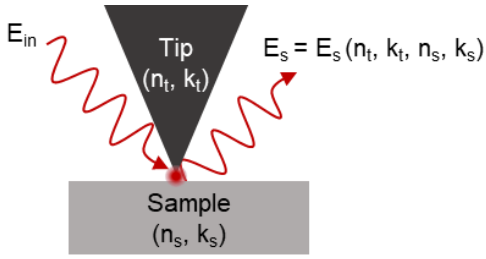

Figure 9. Schematic illustration of incoming radiation being scattered of an AFM-tip close to a sample surface

A second method, based on near field forces is called PiFM (Photo-induced force microscopy). Here, instead of detecting optical data to construct the FTIR spectrum, mechanical forces are measured. Two vibrational modes, the vdW force between the tip and sample surface and the PiF (photo-induced force) are measured independently by modulating the cantilever vibrational modes [47], [48].

The third technique, AFM-IR (atomic force microscope infrared) is based on mechanical forces and the photothermal effect [49], [50]. Molecular vibrations are induced by directing a focused pulsed IR laser source with a tunable wavelength onto a surface. In the fingerprint region this is typically achieved using a QCL source. An AFM probe is then used to detect minute local thermal expansion on the sample surface. By keeping the probe stationary and changing the incoming wavelength, a spectrum can be collected. Conversely, by pulsing the same wavelength and moving the tip across the surface, a chemical map of the intensity of a single band can be collected.

Investigations of the degradation of polymer coatings with nanoscale IR spectroscopy have been reported in a few works.

Morsch et al. 2015 used AFM-IR to map the local degree of crosslinking and local water sorption in epoxy phenolic coatings [8]. On a macro scale, a higher crosslinking in such a glassy highly crosslinked network tends to decrease the polymer density. This is most likely either due to limitations in packing efficiency around crosslink sites or that higher crosslinking pushes the system further from their equilibrium conformation. Local sites, measuring ~50 nm in diameter, showed increased water uptake as well as higher crosslinking density. This indicated that lower polymer density, and a higher amount of empty space, was correlated with higher water uptake.

Morsch et al. 2022 examined local oxidation surrounding buried interphases around iron oxide particles in epoxy amide coatings [51]. To achieve this, they microtomed thin slices of the coating and quantified carbonyl and imine bands at buried interphases using AFM-IR. They concluded that the interphases show signs of degradation before the bulk material during mild thermal aging. Their results agreed with a commonly reported diffusion limited oxidation mechanism, where initiation and kinetics at the buried interphase are controlled by local oxygen transport.

Oancea et al. 2023 compared two protective coatings, a commercial acrylic copolymer and a synthesized nanostructured material, for protection of cultural heritage artefacts [52]. Using data from nano-FTIR, they inferred that functional groups at the polymer-air interface in both coatings had preferential orientations. The changes (and lack thereof) in the preferential orientations with increased weathering times aided them in understanding the degradation reactions. They concluded that the nanostructured material was more suitable to use due to properties such as hydrophobicity, microporosity, and UV-absorption properties.

Weathering

To compare the durability of different organic coatings, either to compare the stability of different systems, or for quality assurance purposes, materials are often tested in an aggressive environment. Then various coating properties linked to degradation are assessed. For coil coatings used in outdoor applications the most important environmental factors to consider are electromagnetic radiation in the UV, visible, and infrared range (‘light’), temperature cycling and humidity in different combinations. In some cases, damaging chemical species can also play a part. The assessment of potential damage is thoroughly discussed earlier in this thesis but in a nutshell, what constitutes damage is application

specific. For instance, a change in color might be detrimental in some architectural applications where aesthetic properties are important. This same change might be irrelevant in applications where a metal surface cannot be seen but needs to be protected from corrosion.

Outdoor weathering

Exposing the coating to an environment like that where it will be used is probably the most accurate, and a very cost-effective, method of weathering. However, to make it easier to compare different exposures there are standardized exposure sites available across the world where the conditions are closely monitored. These sites are meant to represent various climates with different environments with different amounts of solar radiation, rain, humidity, etc. An important parameter when comparing exposure sites is the time of wetness (TOW), or the amount of time a surface remains wet during exposure. For the sake of convenience TOW is usually calculated using meteorological data. According to ISO 9223 it is the time period during which the relative humidity is in excess of 80% and the temperature is above 0 °C. If meteorological data with high temporal resolution is not available TOW can also be approximated with high accuracy using yearly average values of temperature and humidity data [53].

One example of a typical testing site is the deserts of Arizona that show very high UV irradiance, as well as extremely high temperatures with very low humidity. In addition, the samples would also be exposed to thermal stress due to the large temperature differences between day and night. In comparison, exposures in Florida would be representative of a very humid climate with high wetness, whilst still retaining both high UV irradiance and temperatures. Bohus-Malmön at the Swedish west coast is often used to simulate harsh north European climate. This site shows very high precipitation and time of wetness with a comparatively low UV irradiance as well as temperatures below 0 °C during most winters. A coating at Bohus-Malmön will also be exposed to high amounts of salt during exposures due to marine aerosol particle from exposure to winds from the sea.

As incident light can affect the rate at which changes in the coating occurs, it is important to consider the positioning of the samples. Typically, the angle difference from the vertical plane and the cardinal direction at which the sample is directed is reported. An exposure at 45 ° angle facing

due south will experience considerably more light, and thus degrade faster, as compared to a vertical exposure at 90 ° facing due north. Using this principle, it is possible to accelerate the weathering rate by maximizing the amount of incoming light. Some commercially available options are e.g. using mirrors to increase the amount of incoming light and moving the sample so that it is facing the sun for as long time as possible. These are types of accelerated outdoor weathering.

Artificial weathering

Another common way to either increase the weathering rate or isolate specific damaging factors is to use artificial weathering. Generally, artificial weathering consists of an enclosed environment where you have total control over all weathering parameters. Two of the most common artificial weathering methods are QUV, (named after the Q-Lab company), as used in Paper I, and flat bed Xe Arc testing, used in Paper II. To make exposures as comparable as possible there is a range of standards that are designed for different samples.

QUV is generally considered to be the simpler method and tends to be cheaper to run. The weathering chamber consists of a trapezoidal prism, with the top of the chamber sloping inwards (EN13523-10, ISO 4892-3). This sloped wall has square holes where the samples can be fastened, with the surface that should be weathered facing in towards the chamber. There is a heated water bath at the bottom that increases the temperature and causes a high RH (relative humidity) in the chamber. As the backside of the samples are cooled by the conditions outside the chamber a temperature gradient is created. This leads to condensation on the samples. Some QUV-based standards require spray nozzles to the setup to directly apply water. This setup places geometrical limitations on the samples in terms of flatness, unless customized sample holders are used, as the humid air should be kept within the chamber. Different standards prescribe various lamp types, but in general they tend to have emissions focusing on the UV region of the electromagnetic spectra and lack emissions in the visible and infrared region. To control the temperature in the chamber a cooling system is often part of the setup.

In contrast, flat bed Xe arc weathering is a more expensive technique with higher flexibility regarding sample geometry, a wider spectral range, but no option for condensation. Here the samples are placed on a horizontal surface underneath Xe arc lamps, with a considerably wider

spectral range, more similar to the emissions of the sun at ground level. In addition, instead of letting condensation occur on the sample surface, all water added is though spray nozzles placed between the lamps and thus no condensation occurs. However, these Xe arc lamps run hotter, have a shorter lifespans, and require calibration more often as compared to the QUV lamps (ISO 4892-2:2013, ISO 4892-3, 2013 EN13523-10). Schematic setups of QUV and Xe arc flatbed chambers can be seen in Figure 10.

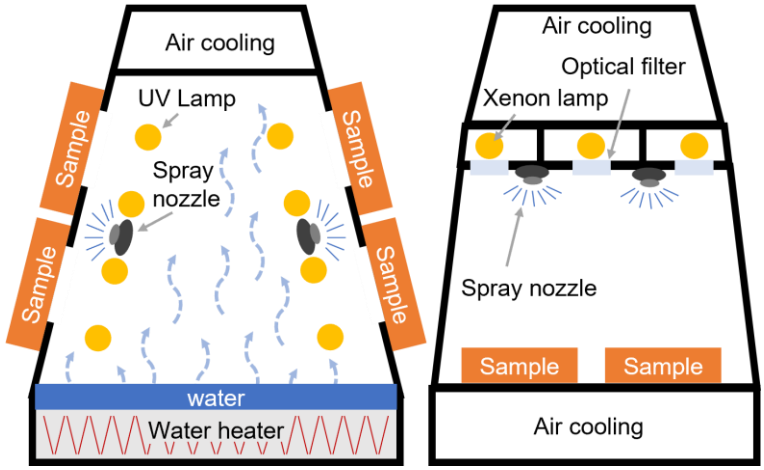

Figure 10. Schematic setup of QUV(left) and an Xe arc flatbed chamber (right)

In summary, both methods entail using a combination of high intensity light, water, and temperature to accelerate the weathering rate of samples. Xe arc uses a light source more like that of solar radiation, whereas QUV mostly mimics the UV part of the spectrum. This can lead to different degradation modes for similar samples exposed to the two techniques, and it has a significant effect on e.g. how the color of a sample affects the sample surface temperature [14]. However, QUV weathering is still a well-used technique that is part of many standards due to its simplicity and lower maintenance requirements.

For coil coatings, as well as polymers in general, the correlation between accelerated and natural weathering is a hotly debated topic [54]–[56]. The general consensus is that one needs to be very careful when interpreting results from accelerating tests in terms of performance in real life situations. Differences between natural and artificial QUV-weathering is discussed in Paper I. There, natural weathering at two different sites is

compared with artificial QUV weathering. However, even though the correlation between natural and artificial weathering is not perfect it is often useful.

Rapidly increasing environmental demands from both legislation and customer are strong incentives to use accelerated weathering methods as they significantly reduce development times. It is a group of useful methods for making quick assessments of new coating formulations and constituents. A shorter pre-study with well thought-out accelerated testing methods could be a great way to reduce large experimental matrices and quickly obtain preliminary results that suggest future development directions. Such an analysis is done in Paper II. Changes in nanoscale mechanical and chemical properties in two simplified clearcoat systems were analyzed before and after accelerated Xe flatbed weathering, demonstrating the viability of the utilization of advanced analysis techniques in coil coating evaluation.

Summary of papers

Materials and methods

Coil coating formulations

For Paper I two commercial topcoat coil coating formulations, denoted "standard" and "biobased" were used. They both consisted of OH-functional resins containing a mix of aromatic and aliphatic polyester, crosslinked with hexa-methoxy methyl melamine (HMMM) in a ratio of 85:15. Pigmentation in the form of carbon black, structuring agents such as polyamide, UV-stabilizers, and solvents were also used. The biobased systems contained a renewable reactive diluent in the form of rapeseed methyl ester (RME). In addition, the polyester resin in this system had a slightly higher aromatic content. Both systems were applied onto hot-dipped galvanized steel substrates with a Ti-based pretreatment and a polyester melamine primer. The biobased samples were added using a wire drawn rod, whereas the standard samples were applied in an industrial coil coating process.

The two clear coats used in Paper II were based on aromatic polyester resin and crosslinked using either hexa(methoxymethyl)melamine (HMMM), resulting in a polyester melamine, or caprolactam blocked hexamethylene diisocyanate (HDI) with a cyclic trimer (CT) core, resulting in a polyester isocyanate, or polyester urethane. The polyester melamine was crosslinked using a polyester:crosslinker ratio of 85:15 and the curing reaction was catalyzed with dodecylbenzenesulfonic acid (DDBSA). The polyester urethane system was crosslinked at a polyester:crosslinker ratio of 80:20 and catalyzed with monobutyltinoxide. Both systems were applied using a wire rod onto HDG steel substrates primed with a chromate free universal polyester primer. Curing was performed in an oven for 34 seconds to a peak metal temperature (PMT) in the range 232 to 249 °C.

Weathering

Artificial weathering was performed either using QUVA cycling based on EN13523-10, for Paper I, or Xe arc flatbed based on ISO 4892-3, for Paper II. QUV cycles consisted of 4h of QUV-A radiation at 60 °C followed by 4 hours darkness and condensation at 40 °C. Xe arc flatbed weathering cycles consisted of recurring cycles consisting of 102 minutes of dry irradiance followed by 18 minutes of water spray without irradiance.

During the irradiation period, a daylight Q filter was used. The black panel temperature was calibrated to 63 °C and the relative humidity 50%.

Natural weathering in Paper I was performed at two different sites. Miami in south Florida, and Bohus-Malmön on the Swedish west coast. Further information about the location and yearly average conditions, including a calculated approximation of TOW is provided in Table 1.

Table 1. Location, yearly average weather data and calculated time of wetness at the Florida and Bohus-Malmön weathering sites

	Atlas' South Florida Test Service, Miami, Florida	*Bohus-Malmön, Kattesand, Swedish west coast*
Latitude	25° 52' N	58°20'N
Longitude	80° 27' W	11°20' E
Elevation (m)	3	40
Distance from Sea (km)	27	0.35
Temperature (C°)	26.7	10.4
Relative humidity (%)	78 %	81.5 %
Precipitation (mm)	1685	802
Solar radiant exposure (MJ/m²)*	6588	3684
*Calculated Time of wetness** (%)*	57	54

*Radiant exposure measured at latitude tilt angle (26° South)
**Calculated using the method from Tidblad et al. [53]

Analysis techniques

IR-based spectroscopic methods

ATR measurements in Paper II were performed using a Bruker Vertex 70 spectrometer with a Specac Quest accessory with a single reflection

diamond IRE. Each background was collected using 512 scans and each spectrum was acquired using 256 scans. The spectral resolution was 4 cm^{-1}. In Paper I, ATR measurements were performed using the MCT detector in a Bruker Hyperion 3000 microscope paired with the same spectrometer. The IRE was a single reflection germanium crystal, and each background and spectrum were acquired using 256 scans at a resolution of 8 cm^{-1}.

FPA measurements were performed using the same Bruker Hyperion microscope setup, with the difference that the FPA detector was used. The array size was 64 × 64 detectors and 2 × 2 binning was used to acquire datasets of 32 × 32 spectra. Backgrounds and spectra were collected using 500 scans.

Photoacoustic measurements (PAS) were performed using a MTEC Model 300 photoacoustic cell. The measurements were performed in continuous rapid scan mode. Four modulation frequencies, 2.5, 5, 10, and 20 kHz, were used with 512, 1024, 2048, and 4096 scans, respectively, to achieve a comparable signal-to-noise ratio. Before each measurement the sample chamber was purged with helium for at least 20 s using a flow rate of approximately 15 cm^3/s.

Nano-FTIR spectroscopy was conducted using a scattering-type scanning near-field optical microscope (s-SNOM) from Neaspec, Attocube systems AG (Germany). Pt:Ir coated silicon AFM tips with nominal tip diameters of approximately 50 nm and resonance frequencies of 240-380 kHz were used. AFM topography and nano-FTIR spectra acquisition were performed using tapping mode. A broadband femtosecond laser with a repetition frequency of 80 MHz and a spectral range of 650 – 2200 cm^{-1} was used to acquire spectra. The output power was approximately 1 mW. Spectra were collected using a working range of 1100 – 1800 cm^{-1}, averaging 10 scans with a 9.8 ms integration time per scan and a spectral resolution of 12 cm^{-1}. To account for various factors, including laser energy fluctuations and absorption in optical components, acquired spectra were normalized to a background spectrum obtained from a reference standard calibration grating for AFM test grating TGQ1 from NT-MDT spectrum systems.

Mechanical analysis

Dynamic mechanical analysis (DMA) was performed on unexposed free-standing films using a TA Instruments DMA Q800. Each sample had the

approximate dimensions of 10 × 9.0 × 0.025 mm and were analyzed at a constant frequency of 1 Hz with a strain set to 0.2 % of the sample length. Equilibration of the films before the start of each measurement was performed for 5 min at -10 °C. After this the temperature was increased at a rate of 3 °C/min up to 70 °C, or until the sample stiffness decreased to the sensitivity level of 100 N/m. The glass transition temperature (T_g) was evaluated at the maximum of the loss factor (tan δ) curve, according to Schesing et al. [57].

Topography and nanomechanical properties were measured using a JPK NanoWizard 3, JPK Instruments AG AFM system. Measurements were performed in the quantitative imaging (QI) mode using a DLC300 probe (Budget Sensors) with a measured 46 N/m spring constant and tip outer radius of 15 nm. The tip radius was determined via an indirect method where the known elastic modulus of polystyrene was evaluated by applying the DMT model (named after Derjaguin, Muller, and Toporov) to a compression-decompression force curve [58].

Optical analysis

Gloss measurements were performed using an Elcometer 408 at 60° for the semi-gloss full system samples in article I and at 15° for the glossy samples in Paper II.

Results and discussion

FTIR analysis

A typical polyester melamine system shows multiple IR-bands that are of interest during degradation studies. Multiple overlapping bands with three distinct peaks can be seen around 2900 cm^{-1}. The band around 2960 cm^{-1} is assigned to CH_3 stretching and the band around 2930 is assigned to CH_2 whereas the band around 2870 cm^{-1} is most likely an overlapping band from both CH_3 and CH_2 stretching [59]–[61]. The combined area of these CH-bands have been used to normalize the wide region of O-H and N-H bands centered around 3300 cm^{-1} when studying photooxidation in many coatings and polymers [12], [62]. The spectra of a typical unexposed polyester melamine sample and a weathered sample are shown in Figure 11. The unexposed reference shows a comparatively small, normalized area of the O-H and N-H bands (blue dotted) as compared to the CH_n-bands (orange striped). After weathering the area of the O-H and N-H bands grow significantly.

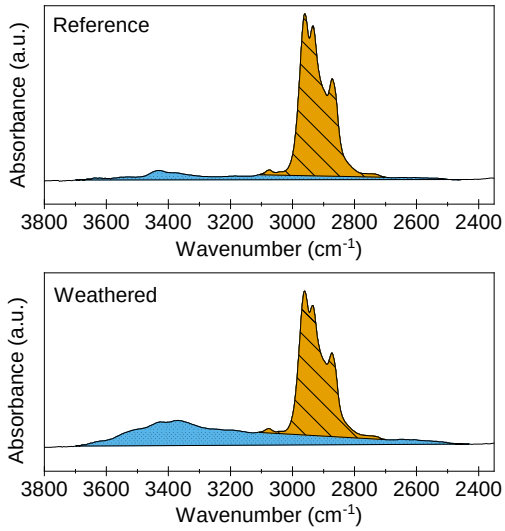

Figure 11. Bands used to calculate the oxidative index of a typical polyester melamine sample before (top) and after (bottom) weathering

The relative increase of this area as measured in percent is commonly defined as oxidative index (OI), photooxidative index (POI), or hydroxyl group band increment (OH%), [12], [63]–[65]. More specifically, this index is calculated from the relative area change before and after degradation using eq. 6.

$$POI = \frac{Ox_{exp} - Ox_{ref}}{Ox_{ref}} \times 100\% \qquad (6)$$

With Ox_{ref} being the normalized area of the O-H and N-H band region before weathering and Ox_{exp} the normalized band area after weathering. Note that the band area for the reference sample in Figure 11 is relatively small, and that the percentage increase is significantly above 100%. This makes the calculation very dependent on the exact peak definitions, as well as any bands that are present in the region before oxidation. This needs to be considered when comparing oxidation of different systems. For example, unweathered polyester isocyanate systems tend to have bands assigned to N-H stretching around 3390 cm^{-1}. This results in a larger reference area and thus a smaller percentual growth of the band region. This in turn reflects a smaller oxidation index for the same amount of band growth. It is possible to partially mitigate this problem by performing peak

fitting calculations to separate the different bands. However, the large amount of wide overlapping peaks in the area makes these calculations complicated and open for interpretation in terms of how to determine the center point for each band. This makes the simpler oxidation index calculations appealing and useful.

A large band at around 1720 cm^{-1} as well as a band centered around 1550 cm^{-1} have been used to quantify degradation in polyester melamine. The former has been attributed to C = O carbonyl ester stretching, whereas the latter has been assigned to the quadrant stretching of the triazine ring in the HMMM as well as contraction of the exogenous N-H bonds, coupled with CH_2 and CH_3 bending vibrations [66], [67]. The effect of weathering on the carbonyl peak has been contested. Bauer et al. 1990 analyzed acrylic melamine and reported an increase in the band after weathering whereas Santos 2007 noted a decrease which he attributed to hydrogen bonding [68], [69]. In addition to analyzing systems with slight chemical differences, seemingly contradictory results are often caused by i) uncertainties in the definition of wavenumber region for the bands, ii) weather intensity or band area should be used, and iii) how the bands are normalized. This makes clear definitions of bands and the performed calculations, preferably alongside illustrations of IR-spectra, important when reporting results. Especially publications from before widespread adaptation of online publications in full color sometimes lack high-definition images of the relevant spectra, which can cause problems when assessing results. A less controversial way of quantifying degradation is the decrease in the band around 1550 cm^{-1}. It is highly sensitive to changes of the methylol groups attached to the triazine ring in the melamine crosslinker and it has been used extensively for quantifying the degradation in polyester melamine thermoset systems [42], [64], [67].

In the articles that form the basis of this this thesis, intensities of the bands at 1550 cm^{-1} and 1720 cm^{-1} were normalized against the relatively stable band around 1375 cm^{-1}, attributed to in-chain C-H deformation with contributions from melamine and side chain modes [67], [70]. Other bands have been used for similar normalizations. For instance, the band around 1450 cm^{-1}, also attributed to C-H bonds but wider and containing multiple overlapping peaks, have been used [11]. However, the 1375 cm^{-1} band was chosen in this work due to proximity to the relevant peaks in terms of wavenumber (especially important in measurements where the information depth is dependent on wavenumber), it is a single relatively

distinct band, and it being comparatively stable thought the degradation process [71]. The three discussed bands as defined in a typical polyester melamine system is shown, before and after weathering in Figure 12. The dotted lines define the baseline, and the solid lines schematically show the definition of the band intensities.

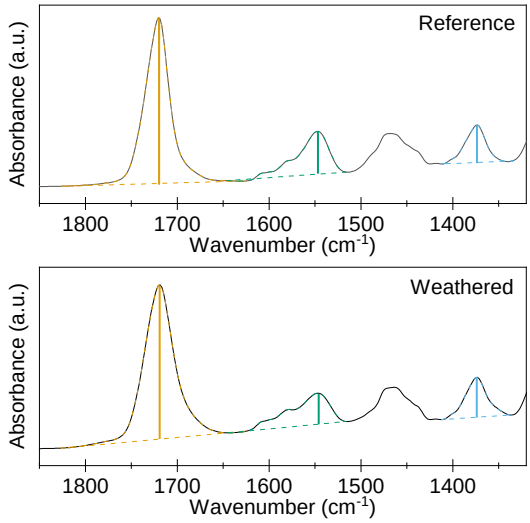

Figure 12. Bands used to calculate the oxidative index of a typical polyester melamine sample before (top) and after (bottom) weathering

Calculations of band intensity reductions are usually performed in a similar manner as compared to POI. However, instead of areas, intensities are normalized in the reference (I_{ref}) and exposed coatings (I_{exp}) and the values in the numerator are switched to retain a positive value of the index. This is shown in eq. 7.

$$Loss\ index = \frac{I_{ref} - I_{exp}}{I_{ref}} \times 100\% \qquad (7)$$

In addition to the above-mentioned bands, during weathering a shoulder is formed around 1780 cm^{-1}. Multiple peaks around this area have previously been connected to coating photodegradation and has been attributed to peracids, peresters, γ-lactones, and anhydrides [64], [72], [73].

A typical polyester melamine spectrum with band assignments is shown in Figure 13. An overview in the region 4000 – 400 cm^{-1} is shown at the top and more detailed views of the OH-region and a part of the polymer fingerprint region are shown underneath. The figure also shows the effect of increased exposure to Xe arc flatbed weathering in increments of 2000 hours, or approximately 80 days.

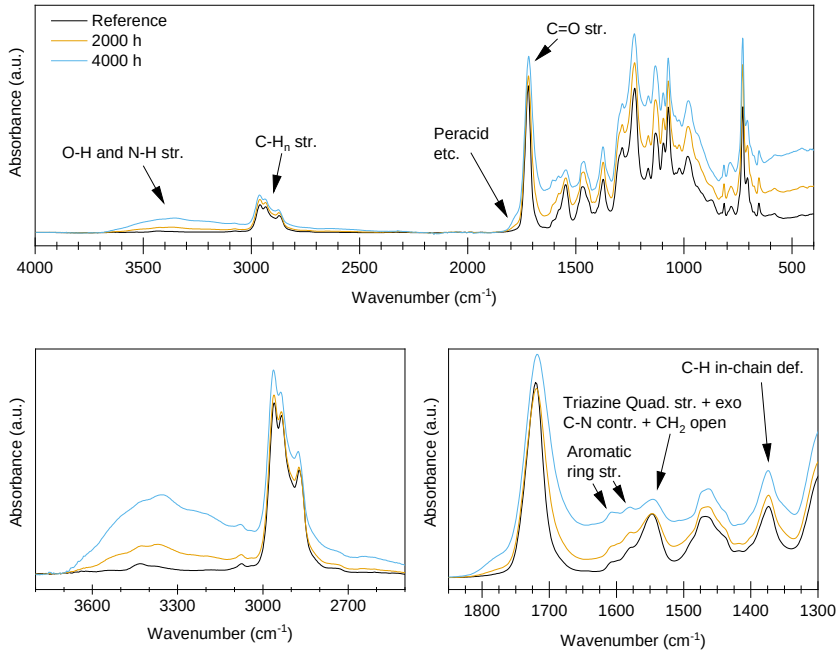

Figure 13. ATR spectra of polyester melamine samples with increasing Xe arc flatbed weathering. The topmost spectra show an overview of the region 4000 – 400 cm^{-1} whereas the ones below show a more detailed view of the region used to calculate oxidation index (left) and the indexes related to the crosslinker and amide bands (right). noteworthy bands are indicated with arrows.

Polyester isocyanate coatings show many similarities to polyester melamine systems. Like mentioned earlier, the same calculations regarding oxidative index can be performed to quantify the oxidation of a weathered coating in comparison to a reference system.

In addition to the C = O carbonyl stretching band around 1720 cm^{-1} there is also a carbonyl band related to the urethane linkages around 1690 cm^{-1}. This band, as normalized against the 1375 cm^{-1} carbon chain backbone band, decreases in intensity with weathering. This has been suggested to

be correlated with the formation of polyurea and a decrease of polyurethane components [10]. Similarly as to polyester melamine coatings, there is also a band from the crosslinker that can be used to quantify crosslinker degradation, the amide II band around 1530 cm^{-1} [67], [74]. The change in intensity of these three bands can also be used in a similar manner as compared to the intensity loss calculations described for the polyester melamine. Figure 14 shows the overview, as well as a zoomed in OH-region, and parts of the polymer fingerprint region of a typical polyester isocyanate coil coating. The effect of increasing times of Xe arc flatbed weathering is also shown.

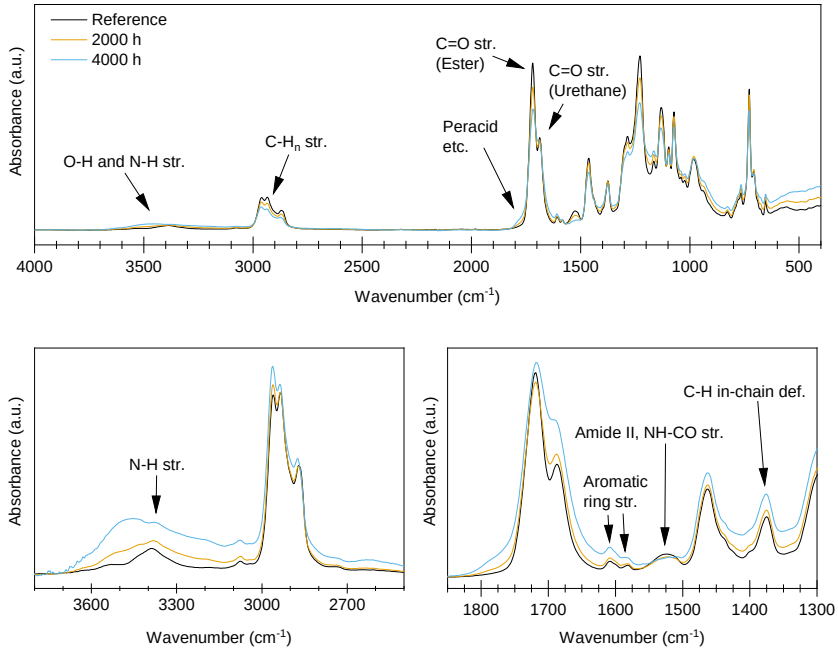

Figure 14. ATR spectra of polyester isocyanate samples with increasing Xe arc flatbed weathering. The topmost spectra show an overview of the region 4000 – 400 cm^{-1} whereas the ones below show a more detailed view of the region used to calculate oxidation index (left) and the indexes related to the crosslinker and amide bands (right). Noteworthy bands are indicated with arrows. The NH-stretching band in the OH region shown in the bottom left image is present before weathering which affects calculations of the oxidation index.

Depth resolved analysis of pigmented coatings

FTIR-FPA-ATR can be used to acquire a hyperspectral image of a coating cross section. However, in a 20 µm topcoat you are limited by the lateral resolution of the measurement and the risk of scratching the ATR crystal at the polymer-metal interface. To get around this Persson et al. 2020 used a high angle coating drill, usually used to determine coating thickness, to open up a cross section [42]. Using a 5.7 ° angle drill results in increased size of the cross section by an order of magnitude ($20\ \mu m\ /\ \tan^{-1}(5.7°) \approx 200\ \mu m$). A schematic view of a drilled cross section of a typical coil coating is shown in Figure 15. The left side shows a view from the top whereas on the right a schematic side view, indicating the site where FPA measurements and some other relevant measurements were performed.

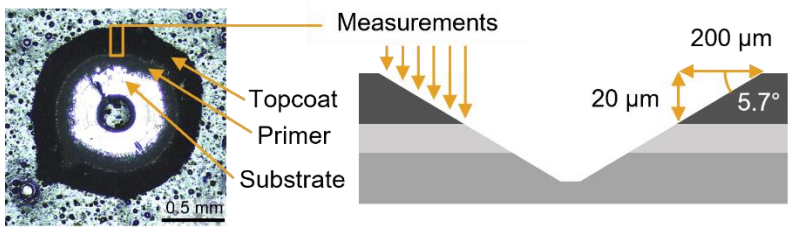

Figure 15. Top view of a conical drill hole collected using an optical microscope and a side view of the system showing the location of the FPA measurements as well as relevant dimensions and angles.

Using an IRE with a high refractive index decreases d_p and lowers the signal to noise ratio, but it also makes sure that the signal only comes from the outermost layer of material. This is important when aiming to acquire depth resolved information. A germanium IRE with a refractive index of 4 used in the typical Bruker Hyperion 3000 setup results in an approximate d_p of 0.6 µm around 1550 cm^{-1}. Using diamond instead of germanium approximately doubles this penetration depth.

Drill holes were made in two different types of coatings, a “standard” system and a “biobased” system with added RME and a slightly modified polyester matrix. The effect of three different weathering scenarios were compared by calculating the decrease in the normalized 1550 cm^{-1} band, denoted loss of melamine functionality (MSFL) across the cross sections. The standard systems exposed to different weathering scenarios are shown in Figure 16 whereas corresponding results from the biobased samples are shown in Figure 17. The reference band intensity was determined using the

average of the entire unexposed cross section. Note that the band intensity varied very little across this cross section. This is the result of homogeneous spread of the melamine crosslinker and has been seen during similar measurements [36], [42].

The standard samples showed approximately 40 % to 60 % degradation in the outermost surface layer, meaning the first few μm into the coating (or a few tens of μm across the cross section). Artificial QUV weathering for 2000 hours, or approximately 80 days, showed similarly high degradation levels as compared to those weathered in Florida for 2 years. The weathering performed on Bohus-Malmön on the Swedish west coast over a period of three years resulted in lower levels of degradation at the surface, and further into the bulk of the coating the degradation is significantly lower. At approximately 10 μm into the coating the degradation index is below 10 % for both QUV accelerated weathering and the exposures at Bohus-Malmön. However, this far into the coating the exposures in Florida resulted in more degradation. It is not surprising that exposure at Bohus-Malmön results in lower degradation levels, even though the exposure time was longer. The amount of incoming radiation over two years in Florida is higher than that over three years in Bohus-Malmön as seen in Table 1. In addition, the average temperature, which generally increases the rate at which chemical reactions occur, is considerably higher in Florida. Bohus Mamlön often shows temperatures below freezing during winters that has the potential to damage the coating by means of freezing (and subsequent expansion) of water inside of the coating, but this appears to have no large effect on the chemical state of the coating. The difference between QUV and Florida is interesting. Although the degradation levels at the surface are similar, the degradation seems to be worse further into the coating for the Florida exposures. This could possibly be due to damaging air pollutants or other substances such as chloride ions from the Atlantic. An alternative, and probably more likely, explanation would be that the significantly longer exposure allowed larger water ingress. The increased availability of water inside the coating could then affect the chemical reactions occurring during the exposure. Regardless of the reason behind the degradation profile, it demonstrates the importance of depth resolved measurements as the surface is not necessarily indicative of the state of the bulk of the coating.

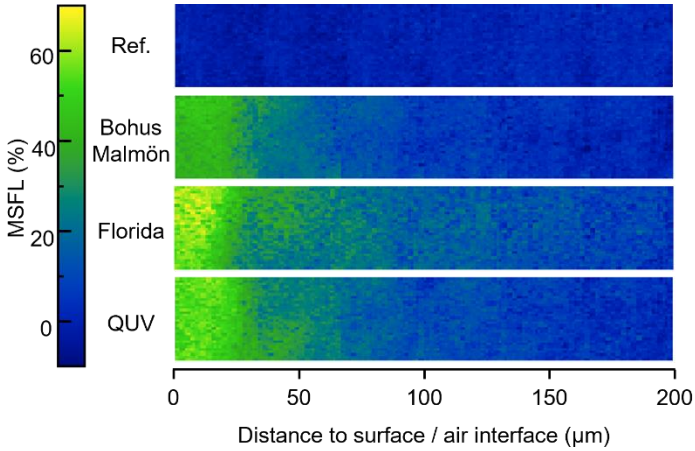

Figure 16. MSFL values obtained by FTIR-ATR FPA imaging in drilled holes for the standard polyester melamine coating. From top to bottom, the images show the unexposed reference sample, samples weathered at Bohus-Malmön, in Florida, and samples exposed to accelerated QUV weathering.

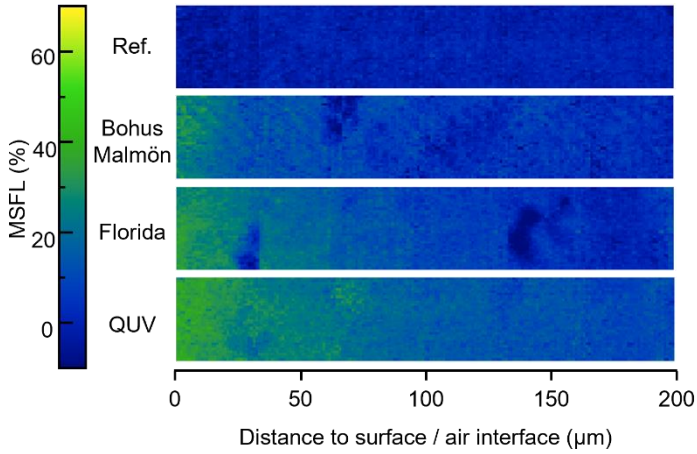

Figure 17. MSFL values obtained by FTIR-ATR FPA imaging in drilled holes for the biobased polyester melamine coating. From top to bottom, the images show the unexposed reference sample, samples weathered at Bohus-Malmön, in Florida, and samples exposed to accelerated QUV weathering.

The biobased polyester melamine coating showed a considerably lower degradation index than the standard coating close to the surface, with only 30-35% for weathering using QUV and weathering in Florida. The samples

weathered at Bohus-Malmön show just above 10% degradation. This points towards the biobased formulation being comparatively well optimized for a Nordic environment. However, in contrast to the other system, the QUV weathering seemed to have a larger degradation index across the entire cross section as compared to exposures in Florida. These results also highlight that there are differences between QUV artificial weathering and outdoor weathering and supports the general academic and industrial consensus [54]–[56]. In addition to the degradation profiles, these measurements also showed the presence of polyamide particles, the darker blue areas in the samples exposed in Florida and at Bohus-Malmön. The reason they show a lower MSFL as compared to the surrounding areas has nothing to do with the local degradation but rather that the amide peaks interfere with the determination of peak height. Polyamides show bands around 1640 cm^{-1} (amide I) and 1540 cm^{-1} (amide II) [59], [67]. This interferes with the intensity measurements of the band at 1550 cm^{-1}.

To make the comparison between systems easier, the same data as presented in Figure 16 and Figure 17 are shown in the form of scatter plots in Figure 18. Each point shows the average MSFL value in depth increments of approximately 1.7 µm, with the error bars showing the standard deviation within this area.

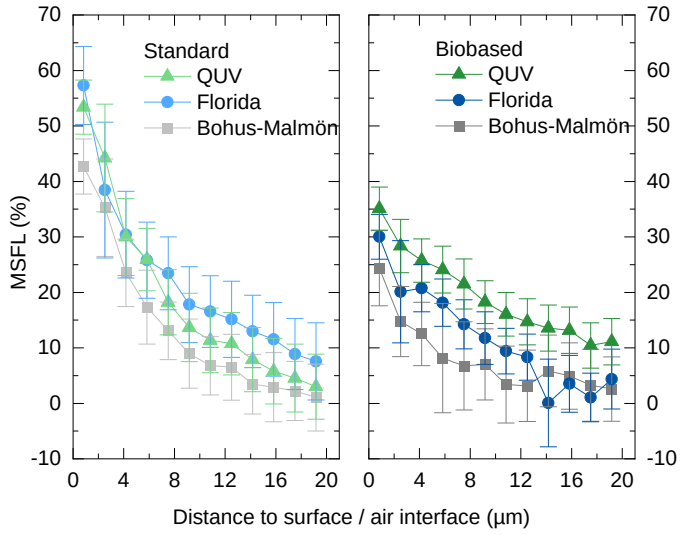

Figure 18. MSFL values as a function of depth into the topcoat as obtained by FTIR-ATR FPA imaging in drilled holes.

To verify the results, PAS measurments on the same samples were conducted. Measurements were performed with modulation frequencies of 2.5, 5, 10, and 20 kHz resulting in theoretical sampling depths of 12.9, 9, 6.5, and 4.6 µm at 1550 cm^{-1}. Degradation indices for the different modulation frequencies and the corresponding theoretical sampling depths are shown in Figure 19. Note that since the volume from which the data is collected is larger, the MSFL as a function of depth obtained by PAS is flattened compared to that obtained by FPA. The measurements designed to have low penetration depths have contributions from volumes deeper into the sample and the measurements designed to have a larger penetration depth show contributions from both the surface and positions deeper into the bulk.

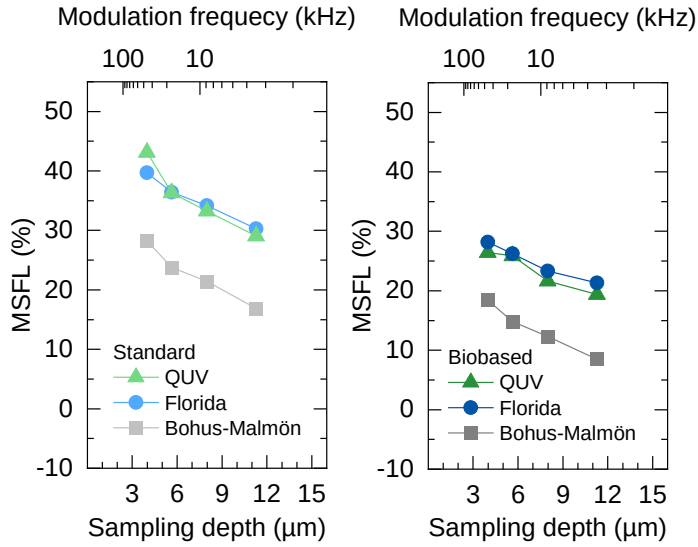

Figure 19. MSFL values obtained by PAS as a function of sampling depth

In summary, we were able to demonstrate how an IR-based method requiring relatively low amounts of sample preparation could be used to acquire spatially resolved data pertaining to the degradation of an organic coil coating cross section. Using this information, we identified differences between two different coatings in how the degradation in the bulk related to the degradation in the surface layer. In addition, we were also able to see

differences between the degradation behavior from natural and artificial QUV weathering.

Surface measurements of clearcoats

AFM-based measurements have high spatial resolution and can be performed with very limited sample preparation in different environmental conditions. Nanomechanical measurements using an AFM can be used to determine the local mechanical properties with a resolution on the nm-scale. The chemistry of the system was analyzed using both s-SNOM with a resolution like that of the nanomechanical measurements, as well as conventional FTIR-ATR. Two clear coat systems, polyester melamine and polyester isocyanate, were analyzed before and after Xe arc flatbed weathering. Nanomechanical and s-SNOM measurements were performed on samples that were unweathered and had been exposed for 2000 hours. For each sample three areas were analyzed. In addition, FTIR-ATR measurements were performed at regular intervals.

Typical retraction curves showing the behavior of the polyester melamine surface before and after 2000h hours of Xe arc weathering is shown in Figure 20. At the top, orange and red curves show two typical behaviors before exposures. Note the increased noise at around 10 to 15 nm in the top right graph. This could be indicative of either bridging or capillary forces between the surface and the AFM-tip. The two blue curves show the retraction behavior after weathering. The range of the attractive forces have halved from around 10 nm to around 5 nm. This is likely due to changes in the length of polymeric chains that are present on the surface. A summary of the polyester melamine nanomechanical properties is shown in Table 2 and Table 3.

The retraction curves of the polyester isocyanate samples showed trends similar to those in the polyester melamine samples. A decrease in the range of the attractive interactions after weathering and signs of bridging or capillary forces both before and after weathering. In addition, a large variation between the adhesion values between the different sites can be seen for the polyester isocyanate reference samples. Two sites show extremely low average adhesion values whereas a third shows a value closer to those of the polyester melamine samples. These values are shown in Table 4. Since the other nanomechanical properties show no such spread, the adhesion values are most likely not derived from a separate phase such as surface contamination. This means that the result is most likely brought on by nm, or sub-nm scale roughness. Because of this no

definite conclusion could be drawn from the adhesion properties. The nanomechancal properties of the polyester isocyanate samples are summarized in Table 4 and Table 5.

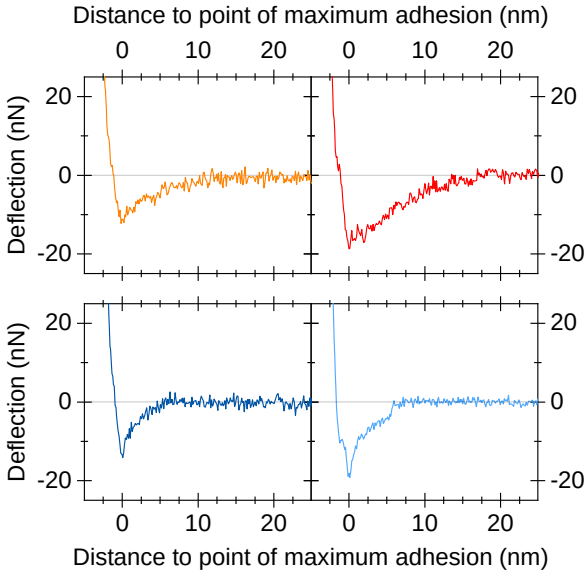

Figure 20. Typical decompression curves for the polyester melamine samples. Red and orange curves on the top show the behavior of the unexposed reference and the dark and light blue curves at the bottom show the behavior of the weathered areas.

In both systems, weathering leads to an increase in stiffness and a decrease in deformation. These changes are related as a harder coating deforms less with an unchanged applied force. In addition, weathering seems to homogenize the sample, decreasing the variation between the different measurement sites, as well as the standard deviation inside each site. This could be due to the removal of surface inhomogeneities in the form of mechanically sensitive areas with low degrees of crosslinking, or convex peaks. Note that the effect is very local, on the scale of 1 × 1 µm, and that a clearcoat is being examined. Biggs et al. 2001 examined topography of coil coating before and after weathering and found a significant increase in RMS surface roughness [24]. However, they examined larger areas, 40 × 40 µm and used full systems. They suggested that the increase in roughness was mostly due to erosion of the coating, exposing stable

pigmentation particles, and the pigmentation falling out of the coating, leaving holes.

Table 2. Summary of nanomechanical properties of the surfaces of the unweathered polyester melamine.

	RMS (nm)	*Stiffness (N/m)*	*Deformation (nm)*	*Adhesion (nN)*
*Reference I**	1.8	38.2 ± 6.5	3.9 ± 1.0	19.8 ± 1.4
Reference II	1.3	38.1 ± 5.8	3.8 ± 1.3	20.1 ± 1.8
Reference III	2.6	45.1 ± 4.9	2.5 ± 0.5	16.6 ± 2.1
Mean	1.9 ± 0.5	40.5 ± 10.3	3.4 ± 1.6	18.8 ± 3.3

* Shown in Figure 21

Table 3. Summary of nanomechanical properties of the surfaces of the weathered polyester melamine.

	RMS (nm)	*Stiffness (N/m)*	*Deformation (nm)*	*Adhesion (nN)*
*Weathered I**	1.8	47.6 ± 4.7	2.2 ± 0.2	14.8 ± 1.2
Weathered II	0.64	46.5 ± 4.3	2.2 ± 0.2	14.1 ± 1.3
Weathered III	0.52	46.0 ± 3.7	2.3 ± 0.2	15.5 ± 1.3
Mean	1.0 ± 0.6	46.6 ± 7.4	2.3 ± 0.3	14.8 ± 2.2

* Shown in Figure 21

In Figure 21, spatially resolved maps of nanomechanical properties in reference area I is compared to weathered area I. In addition, histograms displaying the topography, stiffness, deformation, and adhesion before and after weathering is shown. Both spatially resolved maps and histograms describing the spread of each property are shown. The histograms confirm that weathering increases the stiffness and decreases the deformation.

They also show that the variation decreases and the relative frequency of the median values for the properties increase. Note that although the stiffness and deformation are closely related, which is why the maps show similar features, in terms of a lower stiffness and more deformable area to the left, there is no linear correlation between the properties. This is why the decrease in spread of the deformation is significantly larger as compared to the stiffness.

Table 4. Summary of nanomechanical properties of the surfaces of the unweathered polyester isocyanate.

	RMS (nm)	*Stiffness (N/m)*	*Deformation (nm)*	*Adhesion (nN)*
Reference i	0.94	31.0 ± 2.9	3.9 ± 0.5	5.8 ± 1.7
Refenrece ii	0.91	33.5 ± 3.5	3.9 ± 0.6	6.2 ± 1.9
Reference iii	1.66	32.5 ± 3.9	3.9 ± 0.5	20.7 ± 2.9
Mean	1.17 ± 0.35	32 ± 6.0	3.9 ± 1	10.9 ± 4.9

Table 5. Summary of nanomechanical properties of the surfaces of the weathered polyester isocyanate.

	RMS (nm)	*Stiffness (N/m)*	*Deformation (nm)*	*Adhesion (nN)*
Exposed i	0.57	44.8 ± 4	2.4 ± 0.2	17.8 ± 1.4
Exposed ii	0.77	45.6 ± 3.6	2.4 ± 0.2	18.8 ± 1.5
Exposed iii	0.57	44.1 ± 3.4	2.5 ± 0.2	18.5 ± 1.5
Mean	0.63 ± 0.09	44.8 ± 6.4	2.4 ± 0.3	18.4 ± 2.5

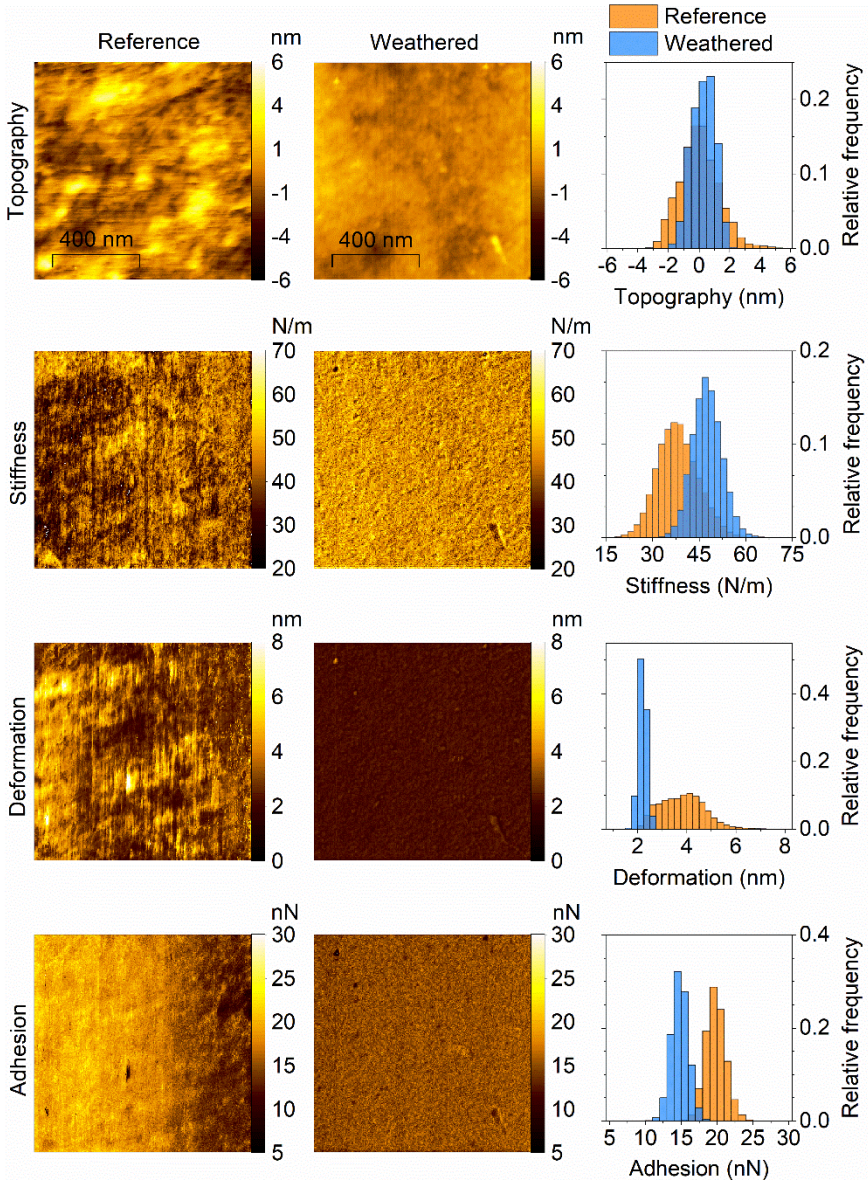

Figure 21. Topography, stiffness, deformation, and adhesion of one of the polyester melamine surfaces measured in air. From left to right, the columns show images of a reference surface, images after 2000 hours of Xenon arc chamber exposure, and the distribution of nanomechanical properties of these two areas. The area of each map is 1 × 1 µm².

In terms of chemical changes, multiple signs of degradation could be seen using ATR. Figure 13 show the changes that occur in the spectra over a larger timescale, 2000 and 4000 hours of xenon arc exposure. A quantified summary of changes in the spectra as summarized using degradation indices is shown in Figure 22. The indices include POI, as described earlier, the intensity growth of the band around 1780 cm^{-1}, indicating growth of peracids, peresters, γ-lactones, and anhydrides (shortened to "peracid index"), the decrease in the carbonyl band intensity, and the melamine functionality loss, here denoted crosslinker index. Such changes have previously been correlated with degradation of polyester melamine coatings. However, changes in the carbonyl band are highly dependent on the definition of the band and weather the band intensity or band area is examined. For example, the peracid etc. band around 1780 cm^{-1} partially overlaps with the carbonyl band and can interfere with the baseline definitions. In addition, during band area calculations, the overlap might cause significant measurement artifacts unless appropriate peak fitting calculations are made. This effect is reduced by assessing band intensities, which is why they are used in the assessment of peracids, carbonyl, and crosslinking degradation. Since the many overlapping bands used for the calculations of the oxidative index it is not appropriate to use band intensity for that measurement.

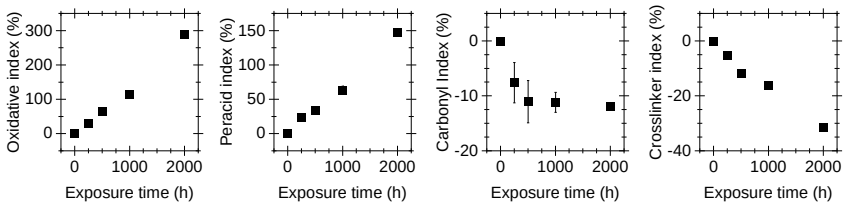

Figure 22. Degradation indices of the polyester melamine system as a function of weathering time.

The calculation of the degradation index for the polyester isocyanate samples were carried out in a similar manner as those presented in Figure 22 with two exceptions. Firstly, the edges of the bands representing the crosslinker degradation were slightly moved to accurately capture the amide II stretch, and secondly a second carbonyl index, owing to the carbonyl bonds within the urethane group was added. In Figure 14 the changes that occur during the degradation, as well as the band locations

are seen. The evolution of the degradation index over 2000 hours of xenon arc exposed polyester isocyanate samples are shown in Figure 23. Just like for the polyester melamine, increased weathering times result in increasing oxidation and the formation of peroxide and other degradation products. The carbonyl band around 1720 cm^{-1}, more specifically 1719 cm^{-1}, for these samples, slowly decreases but shows signs of stabilizing. While this decrease in intensity may occur due to loss of carbonyl bonds it is more likely due to changes of the surroundings of the carbonyl bond. For example, the chemical surroundings of the functional group that the carbonyl bond is part of, or a reaction that entirely changes the functional group. Yang et al. 2001 suggested that a decrease in the 1720 cm^{-1} carbonyl band and the increase to the 1687 cm^{-1} band could be to the decrease of polyurethane components and formation of polyurea [10]. Whereas the polyester melamine crosslinker index showed a decrease even for short exposure times the polyester isocyanate remains relatively stable for the first 500 hours of exposure time after which it starts to decrease.

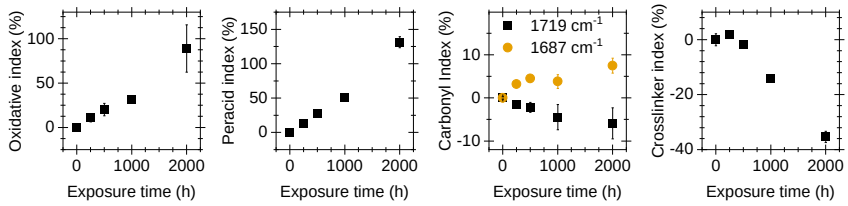

Figure 23. Degradation indices of the polyester isocyanate system as a function of weathering time.

FTIR-ATR measurements collected data from a relatively large area, on the scale of hundreds of µm, and with an information depth of about 1 µm around the relevant bands. In contrast, the Nano-FTIR sampling area probes much smaller surface area, with a lateral resolution around 50 nm (a diameter of the cantilever), and an information depth in the order of hundreds of nm [75], [76]. Thus, it probes the surface chemistry on a much more local scale.

The nano-FTIR method was used to study changes of the melamine band around 1550 cm^{-1}, as well as the carbonyl band to obtain an insight into changes occurring on the nanoscale. A topographical map of an unweathered (top) and 2000 hour Xe arc weathered area is shown in Figure 24. The nano-FTIR spectra are color coded with the color of the

square in the topographical map corresponding with the color of the collected spectra. In addition, a typical spectrum from the ATR measurements is shown as a dotted gray line. Good correlation of the nano-FTIR and ATR FTIR spectra profiles indicate complementarity of these methods. Note the minor artefacts in the nano-FTIR spectra in the form of oscillations in the spectra around 1650 cm^{-1} and 1690 cm^{-1}. The oscillations are deemed artefacts due to the variations in shape and peak location. The variations are especially clear when comparing spectra from different areas as shown in the supplementary information in Paper II.

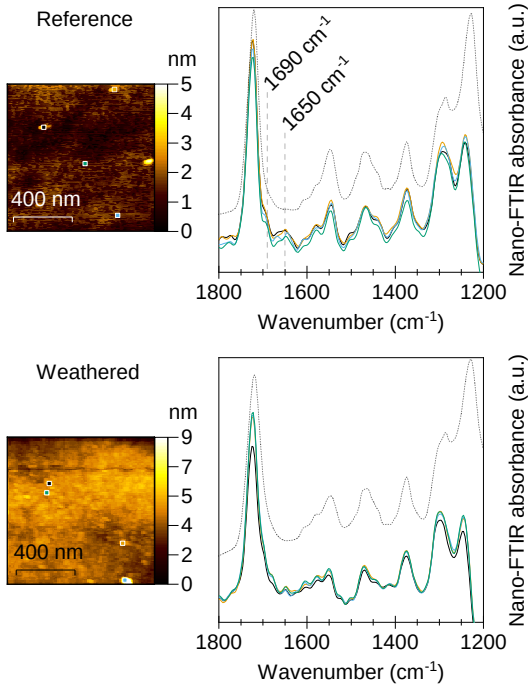

Figure 24. Topography and nano-FTIR spectra from the reference (top) and weathered (bottom) polyester melamine samples. The dotted line indicates the FTIR-ATR spectra from the same exposure time.

Note that the normalized band intensities generally displayed a significantly larger variation as compared to those acquired using FTIR-ATR. Therefore, due to the large resulting standard deviations degradation indices were not calculated. Even though indexes were not calculated, similar trends as those captured using ATR could be seen. In the polyester

melamine sample, a considerable decrease in the 1550 cm^{-1} band, as well as a minor decrease in the carbonyl band (both normalized against the band at 1375 cm^{-1}) could be detected. This is shown in Figure 25. Even though a nanoscale variation in chemistry can be discerned, the chemistry seems to be relatively homogeneous within the analyzed size scale. In addition, no correlation between topographical features and the spectra could be discerned. This is expected seeing as the clearcoats do not have pigmentations or additives with different chemistries to be detected. In addition to this, inhomogeneities could also act as initiation points for degradation, or ingress points for water.

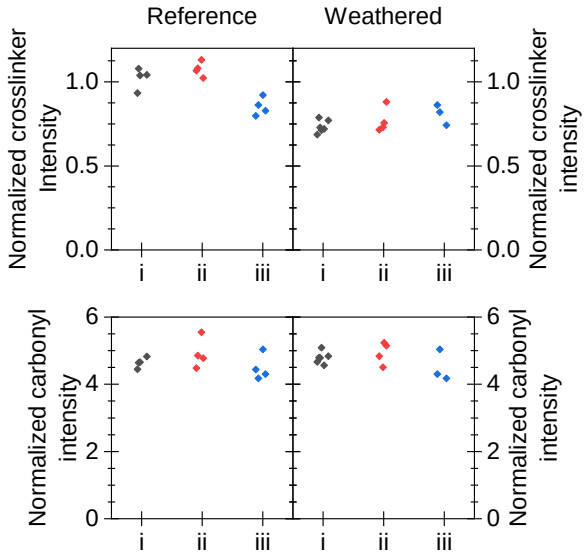

Figure 25. Normalized band intensities of the 1550 cm^{-1} and the 1720 cm^{-1} bands before and after weathering from nano-FTIR measurements. Normalized band intensities from nano-FTIR measurements of the 1550 cm^{-1} melamine and the 1720 cm^{-1} carbonyl band before and after 2000 hours Xe arc weathering.

As shown in Figure 26, the normalized nano-FTIR band intensities from the polyester isocyanate samples also saw similar trends upon Xe arc weathering as compared to the ATR measurements. However, the amide II band around 1530 cm^{-1} showed a significantly higher spread between the measurements as compared to the 1550 cm^{-1} band in the polyester melamine. This is because the band intensity is lower, relatively close to the level of the oscillation artefacts. In addition, these oscillations made

determinations of the base for the band more complicated. It is generally good practice to avoid altering the definition of band baselines unnecessarily as it might introduce data processing errors. When customizing the baselines individually for each spectrum, the spread between the crosslinker intensity values decreased, but it also introduced a measurement error. Because of this, the band definition was kept constant for all reference samples.

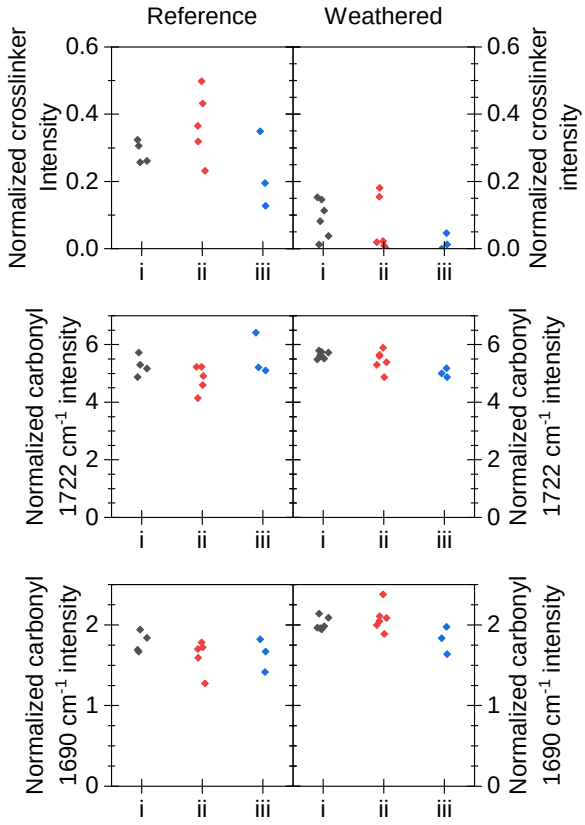

Figure 26. Normalized band intensities from nano-FTIR measurements of the 1530 cm⁻¹ amide II band and the 1690 and 1720 cm⁻¹ carbonyl bands before and after 2000 hours Xe arc weathering.

The polyester isocyanate samples showed no clear change in intensity of the 1722 cm^{-1} carbonyl band in the nano-FTIR measurements. This stands in contrast to the ATR measurements which saw an approximately 5 % decrease in intensity. It is possible that this is due to a difference in probing depths between the two techniques, where the degradation effects in the carbonyl peak are more visible further into the coating, and thus more obvious for an ATR measurement. However, it is more likely that the difference is an effect of the higher sensitivity of the ATR-measurements and the larger spread of the nano-FTIR measurements. However, the increase in the 1690 cm^{-1} carbonyl band is more obvious and corresponds well with the results acquired from the ATR measurements. The band increase is also larger, approximately 7 %.

Overall, the spectra acquired using nano-FTIR were very similar as compared to those obtained from ATR measurements, which is in line with other studies. In addition, quantitative measurements of band intensities before and after weathering showed the same trends for ATR and nano-FTIR. This demonstrates the utility of nano-FTIR usage in the field of coating degradation, making way for further research with nanoscale resolution. For example, spatially resolved analysis of variation of chemical properties around inhomogeneities such as pigmentation, or defect initiation points.

Conclusions

In summary, this thesis showacse the utility of three spatially resolved advanced characterization techniques for the analysis and quantification of coil coating degredation. The techniques are meant to form a basis for the development of a widly applicable degredation-characterization methodology. Care has been taken to limit the complexity of the measurement procedures by for example minimizing sample preparation to maximize the industrial applicability of the thesis. Nano-, micro-, and maco-scale properties have been compared and used as a basis for a discussion on differences between coating systems, as well as between weathering methods.

By combining a commectially avalible FPA imaging system with a simple drill, depth resolved infrared spectra could be gathered. This was used to determine chemical degredation profiles in two different coating systems, exposed to both artificial and natural weathering scenarios. In addition, the method had a high enough resolution to distinguish different chemical constituents in the coating. The different, yet relativley similar coating formulations showed a significat difference in the relationship between the degredation at the surface and in the bulk. This demonstrated the importance of not relying on data from surface-specific techqiues when analysing coating degredation, which is common. In addition, differences between the degradation scenarios highlighted the need for depth resolved chemical information when chosing between already available accelerated weathering methods, or developing new ones for special applications. The FPA-drilling method was shown to correlate well with results from other, more well-established techniques.

Analysis of simplified clearcoat systems using AFM and nano-FTIR showed that from a mechanical point of view, weathering resulted in a local homogenization of the coating on the scale of a single μm^2. The local stiffness increased and the variation in stiffness between different areas decreased. In addition, weathering led to a decrease in the range of adhesive forces. This indicated that the length of loose polymer chains present on the unexposed reference samples decreased after weathering exposures. Changes in band ratios as quantified using both nano-FTIR and conventinal ATR showed similar trends, and confirmed the utlity of nano-FTIR for quantification of degradation using band ratios. Both nanoscale mechanical and IR-based measuremetns are shown to be promising tools to analyze coating degredation.

Further research

The continuation of this project will contain more detailed analysis of full industrial coil coating systems with the goal of further expanding on correlations between nano- micro- and macro-scale properties. The role of pigmentation in the degradation process, both in terms of local and global effects will be considered.

Analysis of interfacial regions with nanoscale spatial resolution will be of special interest. Both interfaces present within the coating (e.g. between pigmentation and the coating resin) and between the coating and the metal substrate could have a big impact on the coating properties. To be able to make these analyses, sample preparation techniques might require further refinement. Especially techniques for uncovering cross sections without smearing or otherwise damaging the interfaces. A promising candidate for this is ion milling techniques such as broad ion beam milling.

Macro scale barrier properties of coil coatings will be quantified using EIS and correlated with the nano-scale properties of the interfaces. It is likely that a less tightly bound, and more degraded interface will correlate with lower barrier properties.

In addition, coating moisture uptake is of interest. Both how global properties (e.g. uptake of water per surface area and how weathering impacts hydrophilicity of a surface) as well as local properties (such as how the state of different interfaces and presence of other features such as differences in crosslinking density) affect the local water uptake.

Topographic analysis on different size scales, comparing measurements of small areas, as presented in Paper II with larger roughness measurements, and correlating these with changes in gloss could yield interesting results. It is known that millimeter scale roughness is different to roughness on the nanometer scale in many respects. It is possible that weathering has different effects on these different scales.

Another relatively unexplored field is comparisons between the already introduced s-SNOM-based nano-FTIR analysis and an alternative technique, AFM-IR. Although they are both techniques that collect chemical information using IR radiation with the resolution of an AFM tip, they work in fundamentally different ways. A coil coating with different organic regions, such as the coating resin and the structural agents, as well as different and inorganic constituents, such as pigmentation in the form of different oxides, could be a very suitable test system for such a comparison.

Acknowledgements

I first and foremost want to thank my (maybe unusually large) team of supervisors. Dr. Dan Persson at RISE who somehow always manages to provide the tools to steer me in the right direction whenever I'm about to veer of course. Professor Magnus Johnson for generously sharing his time and knowledge. Professor Emeritus Per Claesson at KTH for not only helping me answer hard questions but also to ask the right ones. In addition, Camilla Edvinsson who even though she no longer works at RISE continues to support and inspire me with incredible warmth and genuine interest in our field.

I also want to thank all my wonderful colleagues at RISE who supported me and always helped me out whenever I needed it. Especially Illia Dobryden who has gone above and beyond with helping me with both practical work in the lab and maybe more importantly, making sure I understand and can process what is going on during our measurements.

In addition, I want to thank my coauthors and collaborators, Per-Erik Sundell and Golrokh Heydari at SSAB, Tomas Deltin at Nordic United Coatings for providing much needed support and for generously sharing extensive knowledge from their respective fields. Nikolay Kotov who has provided generous help with high spatial resolution and Rosella Telaretti Leggieri who helped me see the large picture.

A special mention also goes out to my dear (now ex-) office mates. Alice, Erik, and Salil. Thank you for supplying welcome distractions during the most tiering of writing sessions.

I would also like to express my gratitude to my parents and brother who have provided non-conditional love and support throughout my entire life and without them I would never be where I am today. Lastly, I would like to thank Hanna for always being there for me and making every single day better and our dog Svante for being the reason I get up in time every morning.

Funding acknowledgements

Swedish Foundation for Strategic Research (SSF) is financially supporting this project through grant FID18-0034.

Bibliography

[1] K. Johansson, T. Bergman, and M. Johansson, "Hyperbranched aliphatic polyesters and reactive diluents in thermally cured coil coatings," *ACS Appl. Mater. Interfaces*, vol. 1, no. 1, pp. 211–217, Jan. 2009, doi: 10.1021/am800036m.

[2] K. Ohlsson *et al.*, "Novel coil coating systems using fatty acid based reactive diluents," *Prog. Org. Coatings*, vol. 73, pp. 291–293, 2012, doi: 10.1016/j.porgcoat.2010.11.018.

[3] N. J. W. Gamage, D. J. T. Hill, C. A. Lukey, and P. J. Pomery, "Thermal characterization of polyester - Melamine coating matrices prepared under nonisothermal conditions," *J. Polym. Sci. Part A Polym. Chem.*, vol. 41, no. 11, pp. 1603–1621, 2003, doi: 10.1002/pola.10698.

[4] M. Korhonen, P. Starck, and B. Löfgren, "Characterization of coil coatings by thermal analysis," *J. Appl. Polym. Sci.*, vol. 87, no. 12, pp. 2016–2022, 2003, doi: 10.1002/app.11702.

[5] D. M. Kroll and S. G. Croll, "Influence of crosslinking functionality, temperature and conversion on heterogeneities in polymer networks," *Polymer (Guildf).*, vol. 79, pp. 82–90, 2015, doi: 10.1016/j.polymer.2015.10.020.

[6] D. M. Kroll and S. G. Croll, "Heterogeneity in polymer networks formed by a single copolymerization reaction: I. Gelation and pre-gel structure," *Polymer (Guildf).*, vol. 115, pp. 154–163, Apr. 2017, doi: 10.1016/j.polymer.2017.03.051.

[7] M. Zee, A. J. Feickert, D. M. Kroll, and S. G. Croll, "Cavitation in crosslinked polymers: Molecular dynamics simulations of network formation," *Prog. Org. Coatings*, vol. 83, pp. 55–63, 2015, doi: 10.1016/j.porgcoat.2015.01.022.

[8] S. Morsch, S. Lyon, S. D. Smith, and S. R. Gibbon, "Mapping water uptake in an epoxy-phenolic coating," *Prog. Org. Coatings*, vol. 86, pp. 173–180, Sep. 2015, doi: 10.1016/J.PORGCOAT.2015.05.017.

[9] S. G. Croll, "Quantitative evaluation of photodegradation in coatings," *Prog. Org. Coatings*, vol. 15, no. 3, pp. 223–247, Dec. 1987, doi: 10.1016/0033-0655(87)85012-4.

[10] X. F. Yang, C. Vang, D. E. Tallman, G. P. Bierwagen, S. G. Croll, and S. Rohlik, "Weathering degradation of a polyurethane coating," *Polym. Degrad. Stab.*, vol. 74, no. 2, pp. 341–351, 2001, doi: 10.1016/S0141-3910(01)00166-5.

[11] W. R. Zhang, S. J. Hinder, R. Smith, C. Lowe, and J. F. Watts, "An investigation of the effect of pigment on the degradation of a naturally weathered polyester coating," *J. Coatings Technol. Res.*, vol. 8, no. 3, pp. 329–342, May 2011, doi: 10.1007/s11998-010-9305-y.

[12] M. A. J. Batista, R. P. Moraes, J. C. S. Barbosa, P. C. Oliveira, and A. M. Santos, "Effect of the polyester chemical structure on the stability of polyester-melamine coatings when exposed to accelerated weathering," *Prog. Org. Coatings*, vol. 71, no. 3, pp. 265–273, Jul. 2011, doi: 10.1016/j.porgcoat.2011.03.009.

[13] R. Narayan, D. K. Chattopadhyay, B. Sreedhar, K. V. S. N. Raju, N. N. Mallikarjuna, and T. M. Aminabhavi, "Degradation profiles of polyester-urethane (hydroxylated polyester/diphenylmethane diisocyanate) and polyester-melamine (hydroxylated polyester/hexamethoxymethyl-melamine) coatings: An accelerated weathering study," *J. Appl. Polym. Sci.*, vol. 97, no. 3, pp. 1069–1081, Aug. 2005, doi: 10.1002/APP.21568.

[14] R. M. Fischer and W. D. Ketola, "Surface Temperatures of Materials in Exterior Exposures and Artificial Accelerated Tests," *Accel. Outdoor Durab. Test. Org. Mater.*, pp. 88–111, 1994, doi: 10.1520/stp18174s.

[15] D. R. Bauer and D. F. Mielewski, "The role of humidity in the photooxidation of acrylic melamine coatings," *Polym. Degrad. Stab.*, vol. 40, no. 3, pp. 349–355, Jan. 1993, doi: 10.1016/0141-3910(93)90141-5.

[16] D. R. Bauer, "Melamine/formaldehyde crosslinkers: characterization, network formation and crosslink degradation," *Prog. Org. Coatings*, vol. 14, no. 3, pp. 193–218, 1986, doi: 10.1016/0033-0655(86)80001-2.

[17] T. Nguyen, J. Martin, E. Byrd, and N. Embree, "Relating laboratory and outdoor exposure of coatings III. Effect of relative humidity on moisture-enhanced photolysis of acrylic-melamine coatings," *Polym. Degrad. Stab.*, vol. 77, no. 1, pp. 1–16, 2002, doi: 10.1016/S0141-3910(02)00070-8.

[18] T. Nguyen, J. Martin, and E. Byrd, "Relating laboratory and outdoor exposure of coatings: IV. Mode and mechanism for hydrolytic degradation of acrylic-melamine coatings exposed to water vapor in the absence of UV light," *J. Coatings Technol.*, vol. 75, no. 941, pp. 37–50, 2003, doi: 10.1007/bf02720521.

[19] K. M. Wernståhl, "Service life prediction of automotive coatings, correlating infrared measurements and gloss retention," *Polym. Degrad. Stab.*, vol. 54, no. 1, pp. 57–65, Oct. 1996, doi: 10.1016/0141-3910(96)00076-6.

[20] D. W. Van Krevelen, *Properties of Polymers*, 4th ed. Amsterdam: Elsevier, 2009.

[21] C. Lowe, S. Ritchie, and G. Foster, "Quantification of moisture absorbed by polyester melamine coil coatings and its effects on mechanical properties," *Coil Coated Steel: Durability, Functionality and Environmental Aspects*. Paris, 2005.

[22] S. Mitra, A. Ahire, and B. P. Mallik, "Investigation of accelerated aging behaviour of high performance industrial coatings by dynamic mechanical analysis," *Prog. Org. Coatings*, vol. 77, no. 11, pp. 1816–1825, 2014, doi: 10.1016/j.porgcoat.2014.06.002.

[23] G. Binning, C. F. Quate, and C. Gerber, "Atomic Force Microscope," *Phys. Rev. Lett.*, vol. 54, no. 9, pp. 930–934, 1986

[24] S. Biggs, C. A. Lukey, G. M. Spinks, and S. T. Yau, "An atomic force microscopy study of weathering of polyester/melamine paint surfaces," *Prog. Org. Coatings*, vol. 42, no. 1–2, pp. 49–58, Jun. 2001, doi: 10.1016/S0300-9440(01)00147-3.

[25] N. A. Burnham and R. J. Colton, "Measuring the nanomechanical properties and surface forces of materials using an atomic force microscope," *J. Vac. Sci. Technol. A Vacuum, Surfaces, Film.*, vol. 7, no. 4, pp. 2906–2913, 1989, doi: 10.1116/1.576168.

[26] E. Thormann, A. C. Simonsen, P. L. Hansen, and O. G. Mouritsen, "Force trace hysteresis and temperature dependence of bridging nanobubble induced forces between hydrophobic surfaces," *ACS Nano*, vol. 2, no. 9, pp. 1817–1824, Sep. 2008, doi: 10.1021/NN800218S/ASSET/IMAGES/LARGE/NN-2008-00218S_0005.JPEG.

[27] J. L. Parker, P. M. Claesson, and P. Attard, "Bubbles, cavities, and the long-ranged attraction between hydrophobic surfaces," *J. Phys. Chem.*, vol. 98, no. 34, pp. 8468–8480, 1994, doi: 10.1021/j100085a029.

[28] R. Evans, "Fluids adsorbed in narrow pores: Phase equilibria and structure," *J. Phys. Condens. Matter*, vol. 2, no. 46, pp. 8989–9007, 1990, doi: 10.1088/0953-8984/2/46/001.

[29] P. M. Claesson *et al.*, "From force curves to surface nanomechanical properties," *Phys. Chem. Chem. Phys.*, vol. 19, no. 35, pp. 23642–23657, Sep. 2017, doi: 10.1039/c7cp02612a.

[30] G. Li, I. Varga, A. Kardos, I. Dobryden, and P. M. Claesson, "Nanoscale Mechanical Properties of Core-Shell-like Poly-NIPAm Microgel Particles: Effect of Temperature and Cross-Linking Density," *J. Phys. Chem. B*, vol. 125, no. 34, pp. 9860–9869, 2021, doi: 10.1021/acs.jpcb.1c04173.

[31] G. Li, I. Varga, A. Kardos, I. Dobryden, and P. M. Claesson, "Temperature-Dependent Nanomechanical Properties of Adsorbed Poly-NIPAm Microgel Particles Immersed in Water," *Langmuir*, vol. 37, no. 5, pp. 1902–1912, 2021, doi: 10.1021/acs.langmuir.0c03386.

[32] Y. He *et al.*, "Nano-scale mechanical and wear properties of a waterborne hydroxyacrylic-melamine anti-corrosion coating," *Appl. Surf. Sci.*, vol. 457, no. May, pp. 548–558, 2018, doi: 10.1016/j.apsusc.2018.06.284.

[33] E. Almeida, M. Balmayore, and T. Santos, "Some relevant aspects of the use of FTIR associated techniques in the study of surfaces and coatings," *Prog. Org. Coatings*, vol. 44, no. 3, pp. 233–242, Jun. 2002, doi: 10.1016/S0300-9440(02)00056-5.

[34] T. Buffeteau, B. Desbat, and D. Eyquem, "Attenuated total reflection Fourier transform infrared microspectroscopy: Theory and application to polymer samples," *Vib. Spectrosc.*, vol. 11, no. 1, pp. 29–36, Mar. 1996, doi: 10.1016/0924-2031(95)00054-2.

[35] P. R. Griffiths and J. A. de Haseth, *Fourier Transform Infrared Spectrometry*. Hoboken, NJ, USA: John Wiley & Sons, Inc., 2007.

[36] T. Hirayama and M. W. Urban, "Distribution of Melamine in Melamine/Polyester Coatings; FT-IR spectroscopic studies," *Prog. Org. Coatings*, vol. 20, no. 1, pp. 81–96, Mar. 1992, doi: 10.1016/0033-0655(92)85006-H.

[37] A. Rosencwaig and A. Gersho, "Theory of the photoacoustic effect with solids," *J. Appl. Phys.*, vol. 47, p. 64, 1976, doi: 10.1063/1.322296.

[38] N. C. Fernelius, "Extension of the Rosencwaig-Gersho photoacoustic spectroscopy theory to include effects of a sample coating," *J. Appl. Phys.*, vol. 51, no. 1, pp. 650–654, 1980, doi: 10.1063/1.327320.

[39] J. F. McClelland, R. W. Jones, S. Luo, and L. M. Seaverson, *A Practical Guide to FT-IR Photoacoustic Spectroscopy*, 1st ed. CRC Press, 1993.

[40] W. R. Zhang, C. Lowe, and R. Smith, "Depth profiling of coil coating using step-scan photoacoustic FTIR," *Prog. Org. Coatings*, vol. 65, no. 4, pp. 469–476, Aug. 2009, doi: 10.1016/j.porgcoat.2009.04.005.

[41] L. Gonon, J. Mallegol, S. Commereuc, and V. Verney, "Step-scan FTIR and photoacoustic detection to assess depth profile of photooxidized polymer," *Vib. Spectrosc.*, vol. 26, no. 1, pp. 43–49, Jul. 2001, doi: 10.1016/S0924-2031(01)00102-3.

[42] D. Persson, G. Heydari, C. Edvinsson, and P. E. Sundell, "Depth-resolved FTIR focal plane array (FPA) spectroscopic imaging of the loss of melamine functionality of polyester melamine coating after accelerated and natural weathering," *Polym. Test.*, vol. 86, p. 106500, Jun. 2020, doi: 10.1016/j.polymertesting.2020.106500.

[43] K. L. A. Chan and S. G. Kazarian, "New opportunities in micro- and macro-attenuated total reflection infrared spectroscopic imaging: Spatial resolution and sampling versatility," *Appl. Spectrosc.*, vol. 57, no. 4, pp. 381–389, 2003, doi: 10.1366/00037020360625907.

[44] A. J. Huber, F. Keilmann, J. Wittborn, J. Aizpurua, and R. Hillenbrand, "Terahertz near-field nanoscopy of mobile carriers in single semiconductor nanodevices," *Nano Lett.*, vol. 8, no. 11, pp.

3766–3770, Nov. 2008, doi: 10.1021/NL802086X/ASSET/IMAGES/LARGE/NL-2008-02086X_0001.JPEG.

[45] T. Taubner, R. Hillenbrand, and F. Keilmann, "Nanoscale polymer recognition by spectral signature in scattering infrared near-field microscopy," *Appl. Phys. Lett.*, vol. 85, no. 21, p. 5064, Nov. 2004, doi: 10.1063/1.1827334.

[46] F. Huth, A. Govyadinov, S. Amarie, W. Nuansing, F. Keilmann, and R. Hillenbrand, "Nano-FTIR absorption spectroscopy of molecular fingerprints at 20 nm spatial resolution," *Nano Lett.*, vol. 12, no. 8, pp. 3973–3978, Aug. 2012, doi: 10.1021/nl301159v.

[47] I. Rajapaksa, K. Uenal, and H. K. Wickramasinghe, "Image force microscopy of molecular resonance: A microscope principle," *Appl. Phys. Lett.*, vol. 97, no. 7, 2010, doi: 10.1063/1.3480608.

[48] D. Nowak *et al.*, "Nanoscale chemical imaging by photoinduced force microscopy," *Sci. Adv.*, vol. 2, no. 3, pp. 1–10, 2016, doi: 10.1126/sciadv.1501571.

[49] A. Dazzi, R. Prazeres, F. Glotin, and J. M. Ortega, "Local infrared microspectroscopy with subwavelength spatial resolution with an atomic force microscope tip used as a photothermal sensor," *Opt. Lett.*, vol. 30, no. 18, pp. 2388–2390, Sep. 2005, doi: 10.1364/OL.30.002388.

[50] J. Mathurin, A. Deniset-Besseau, D. Bazin, E. Dartois, M. Wagner, and A. Dazzi, "Photothermal AFM-IR spectroscopy and imaging: Status, challenges, and trends," *J. Appl. Phys.*, vol. 131, no. 1, p. 010901, Jan. 2022, doi: 10.1063/5.0063902.

[51] S. Morsch *et al.*, "Molecular origins of Epoxy-Amine/Iron oxide interphase formation," *J. Colloid Interface Sci.*, vol. 613, pp. 415–425, May 2022, doi: 10.1016/J.JCIS.2022.01.016.

[52] M. Olaru, A. Oancea, G. Bodi, A. Cernescu, and A. Nicolescu, "Protective coatings for ceramic artefacts exposed to UV ageing," *Res. Sq.*, vol. 7, no. 1, pp. 1–13, Mar. 2022, doi: 10.1038/s41529-023-00343-8.

[53] J. Tidblad, A. A. Mikhailov, and V. Kucera, "Model for the Prediction of the Time of Wetness from Average Annual Data on Relative Air Humidity and Air Temperature," *Prot. Met. 2000 366*, vol. 36, no. 6, pp. 533–540, 2000, doi: 10.1023/A:1026621009635.

[54] J. A. Chess, D. A. Cocuzzi, G. R. Pilcher, and G. N. Van De Streek, "Accelerated Weathering: Science, Pseudo-Science, or Superstition?," *ACS Symp. Ser.*, vol. 722, pp. 130–148, 1999, doi: 10.1021/BK-1999-0722.CH009.

[55] F. Deflorian, S. Rossi, L. Fedrizzi, and C. Zanella, "Comparison of organic coating accelerated tests and natural weathering considering meteorological data," *Prog. Org. Coatings*, vol. 59, no.

3, pp. 244–250, Jun. 2007, doi: 10.1016/j.porgcoat.2006.09.036.
[56] D. A. Cocuzzi and G. R. Pilcher, "Ten-year exterior durability test results compared to various accelerated weathering devices: Joint study between ASTM International and National Coil Coatings Association," *Prog. Org. Coatings*, vol. 76, no. 6, pp. 979–984, 2013, doi: 10.1016/j.porgcoat.2012.10.018.
[57] W. Schlesing, M. Buhk, and M. Osterhold, "Dynamic mechanical analysis in coatings industry," *Prog. Org. Coatings*, vol. 49, no. 3, pp. 197–208, Apr. 2004, doi: 10.1016/j.porgcoat.2003.09.009.
[58] B. V. Derjaguin, V. M. Muller, and Y. P. Toporov, "Effect of contact deformations on the adhesion of particles," *J. Colloid Interface Sci.*, vol. 53, no. 2, pp. 314–326, Nov. 1975, doi: 10.1016/0021-9797(75)90018-1.
[59] L. Irusta and M. J. Fernandez-Berridi, "Photooxidative behaviour of segmented aliphatic polyurethanes," *Polym. Degrad. Stab.*, vol. 63, no. 1, pp. 113–119, Jan. 1999, doi: 10.1016/S0141-3910(98)00073-1.
[60] G. Socrates, *Infrared Characteristic Group Frequencies*, Second Edi. Chichester: John Wiley & Sons, Ltd, 1994.
[61] A. Wärnheim, C. Edvinsson, P. E. Sundell, G. Heydari, T. Deltin, and D. Persson, "Depth-Resolved FTIR-ATR Imaging Studies of Coating Degradation during Accelerated and Natural Weathering-Influence of Biobased Reactive Diluents in Polyester Melamine Coil Coating," *ACS Omega*, vol. 7, no. 27, pp. 23842–23850, Jul. 2022, doi: 10.1021/acsomega.2c02523.
[62] K. Adamsons, "Chemical surface characterization and depth profiling of automotive coating systems," *Progress in Polymer Science (Oxford)*, vol. 25, no. 9. pp. 1363–1409, 2000, doi: 10.1016/S0079-6700(00)00031-9.
[63] F. Posada and J. L. Gardette, "Photo-oxidation of cured fluorinated polymers IV. Photo-oxidation of the fluorinated copolymer network with urethane linkage," *Polym. Degrad. Stab.*, vol. 70, no. 1, pp. 17–29, Jan. 2000, doi: 10.1016/S0141-3910(00)00064-1.
[64] Y. Zhang, J. Maxted, A. Barber, C. Lowe, and R. Smith, "The durability of clear polyurethane coil coatings studied by FTIR peak fitting," *Polym. Degrad. Stab.*, vol. 98, no. 2, pp. 527–534, 2013, doi: 10.1016/j.polymdegradstab.2012.12.003.
[65] J. L. Gerlock, C. A. Smith, V. A. Cooper, T. G. Dusbiber, and W. H. Weber, "On the use of Fourier transform infrared spectroscopy and ultraviolet spectroscopy to assess the weathering performance of isolated clearcoats from different chemical families," *Polym. Degrad. Stab.*, vol. 62, no. 2, pp. 225–234, Nov. 1998, doi: 10.1016/S0141-3910(97)00279-6.
[66] W. J. Jones and W. J. Orville-Thomas, "The infra-red spectrum and

structure of melamine," *Trans. Faraday Soc.*, vol. 55, no. 0, pp. 203–210, Jan. 1959, doi: 10.1039/TF9595500203.

[67] P. J. Larkin, M. P. Makowski, N. B. Colthup, and L. A. Flood, "Vibrational analysis of some important group frequencies of melamine derivatives containing methoxymethyl, and carbamate substituents: Mechanical coupling of substituent vibrations with triazine ring modes," *Vib. Spectrosc.*, vol. 17, no. 1–3, pp. 53–72, 1998, doi: 10.1016/s0924-2031(98)00015-0.

[68] D. R. Bauer, J. L. Gerlock, D. F. Mielewski, M. C. Paputa Peck, and R. O. Carter, "Photo-stabilization and photo-degradation in organic coatings containing a hindered amine light stabilizer: Part IV—Photo-initiation rates and photo-oxidation rates in unstabilized coatings," *Polym. Degrad. Stab.*, vol. 27, no. 3, pp. 271–284, Jan. 1990, doi: 10.1016/0141-3910(90)90011-U.

[69] D. Santos, M. R. Costa, and M. T. Santos, "Performance of polyester and modified polyester coil coatings exposed in different environments with high UV radiation," *Prog. Org. Coatings*, vol. 58, no. 4, pp. 296–302, Mar. 2007, doi: 10.1016/j.porgcoat.2007.01.006.

[70] N. B. Colthup, L. H. Daly, and S. E. Wiberley, *Introduction to Infrared and Raman Spectroscopy*, 3rd ed. London: Academic Press limited, 1990.

[71] Y. Zhang, "A spectroscopic study of the degredation of polyurethane coil coatings," Queen Mary, University of London, 2012.

[72] D. R. Bauer and L. M. Briggs, "IR Spectroscopic Studies of Degradation in Cross-linked Networks," in *Characterization of Highly Cross-linked Polymers*, vol. 243, 1984, pp. 271–284.

[73] N. S. Allen, M. J. Parker, C. J. Regan, R. B. McIntyre, and W. A. E. Dunk, "The durability of water-borne acrylic coatings," *Polym. Degrad. Stab.*, vol. 47, no. 1, pp. 117–127, Jan. 1995, doi: 10.1016/0141-3910(94)00103-F.

[74] W. R. Zhang, T. T. Zhu, R. Smith, and C. Lowe, "A non-destructive study on the degradation of polymer coating I: Step-scan photoacoustic FTIR and confocal Raman microscopy depth profiling," *Polym. Test.*, vol. 31, no. 7, pp. 855–863, 2012, doi: 10.1016/j.polymertesting.2012.07.002.

[75] A. A. Govyadinov, S. Mastel, F. Golmar, A. Chuvilin, P. S. Carney, and R. Hillenbrand, "Recovery of permittivity and depth from near-field data as a step toward infrared nanotomography," *ACS Nano*, vol. 8, no. 7, pp. 6911–6921, 2014, doi: 10.1021/nn5016314.

[76] L. Mester, A. A. Govyadinov, S. Chen, M. Goikoetxea, and R. Hillenbrand, "Subsurface chemical nanoidentification by nano-FTIR spectroscopy," *Nat. Commun.*, vol. 11, no. 1, pp. 1–10, 2020, doi: 10.1038/s41467-020-17034-6.